nature communications

Article

https://doi.org/10.1038/s41467-025-58368-3

Genome-scale CRISPRi screen identifies *pcnB* repression conferring improved physiology for overproduction of free fatty acids in *Escherichia coli*

Received: 26 June 2024

Accepted: 18 March 2025

Published online: 29 March 2025

Check for updates

Lixia Fang[1,2,3], Xueyan Hao[1,2,3], Jie Fan[1,2,3], Xiaolei Liu[1,2,3], Yaru Chen[1,2,3], Lian Wang[1,2,3], Xiaoying Huang[1,2,3], Hao Song[1,2,3] & Yingxiu Cao[1,2,3]

Microbial physiology plays a pivotal role in construction of superior microbial cell factories for efficient biosynthesis of desired products. Here we identify that *pcnB* repression confers improved physiology for overproduction of free fatty acids (FFAs) in *Escherichia coli* through genome-scale CRISPRi modulation combining fluorescence-activated cell sorting (FACS) and next-generation sequencing (NGS). The repression of *pcnB* can enhance the stability and abundance of the transcripts of genes involved in the proton-consuming system, thereby supporting global improvements in membrane properties, redox state, and energy level. Based on *pcnB* repression, further repression of *acrD* increases FFAs biosynthesis by enhancing FFAs efflux. The engineered strain *pcnB*^{i}-*acrD*^{i}-*fadR*$^{+}$ achieves 35.1 g L^{-1} FFAs production in fed-batch fermentation, which is the maximum titer reported to date in *E. coli*. This study highlights the significance of uncovering hidden genetic determinants that confer improved microbial physiology for enhancing the biosynthesis of desired products.

Microbial biosynthesis is the sum of a great variety of highly coordinated metabolisms and physiologies[1], wherein the metabolic wealth offers a vast array of biochemical reactions that can be exploited to synthesize a myriad of commercially valuable products[2,3], whereas the physiological repertoire renders the feasible intracellular microenvironments that facilitate the progression of the desired biological processes[4,5].

Microbial physiologies encompass cellular structure, cell growth, stress response, etc., which are tightly linked to and thus grip all aspects of metabolic processes[5,6]. Firstly, the cell membrane functions as a dynamic permeability barrier, adjusting its composition and properties to coordinate solute transport and balance stress resistance, thereby sustaining nutrient availability and cell viability for metabolic processes[7,8]. Secondly, the cell growth process governs cellular morphology at the single-cell phase, influencing cell shape and space for metabolite accumulation, and at the cell population phase, it controls cell density directly impacting the productivity of the bioprocesses[9,10]. Additionally, internal redox homeostasis involves the balanced transformation of electrons and protons, withstanding oxidative stresses from reactive oxygen species (ROS) generated during metabolisms[11,12]. As such, physiology-oriented engineering holds significant potential for markedly improving microbial biosynthesis due to its intrinsic and profound effects on microbial metabolisms[5,6]. Therefore, it is highly desirable to harmoniously integrate cellular physiologies with metabolisms for constructing a superior microbial cell factory for efficient product biosynthesis.

[1]State Key Laboratory of Synthetic Biology, Tianjin University, Tianjin, China. [2]Frontier Science Center for Synthetic Biology and Key Laboratory of Systems Bioengineering (Ministry of Education), School of Chemical Engineering and Technology, Tianjin University, Tianjin, China. [3]Frontiers Research Institute for Synthetic Biology, Tianjin University, Tianjin, China. e-mail: caoyingxiu@tju.edu.cn

For microbial biosynthesis of free fatty acids (FFAs), which serve as ideal feedstocks for the manufacture of valuable biofuels and pharmaceuticals[13,14], engineers and scientists have already tapped into the power of physiological engineering to enhance biosynthetic efficiency. Rational engineering efforts were exemplified by modulating outer membrane protein *ompF* and *fadL* to increase membrane integrity[15] or engineering the actin cytoskeleton-related genes *clc1* and *sla2* to maintain cell viability[16], which resulted in 53% and 55% increase in FFAs titer, respectively. As examples of non-rational engineering, the transposon random mutant with the disrupted genes related to membrane transport[17], and the directed evolution mutant with increased average lipid length and membrane integrity[18], exhibited up to a 1.2-fold and 5-fold increase in FFAs production, respectively. Additionally, leveraging a semi-rational strategy that combines CRISPRi and omics, the recombinant strain with combinatorial perturbation of genes related to cellular stress responses (*ihfA*, *aidB*, *ryfA*, and *gadA*) achieved a high FFAs titer of 30.0 g L^{-1} in fed-batch fermentation[19]. However, physiological traits involve multiple genes interacting within the cellular network under changing conditions and are intricately regulated at various levels, such as transcriptional regulators and post-transcriptional modifications[5,6]. This complex architecture leaves significant gaps in our understanding of the integral influence of microbial physiologies and poses challenges for optimization through the rational trial-and-error processes, which are labor-intensive and time-consuming[2], or through random mutation or evolution methods, which introduce a vast array of hard-to-track causal and noncausal genetic alternations[4]. Therefore, it is necessary to perform genome-wide identification of genetic determinants that can be re-engineered to enhance physiological homeostasis, thereby establishing functional states to fully unleash microbial biosynthesis potential.

Here we report the identification of *pcnB* repression that confers improved physiology for FFAs overproduction in *Escherichia coli* through genome-scale CRISPRi modulation combining fluorescence-activated cell sorting (FACS) and next-generation sequencing (NGS). We further demonstrate that the repression of *pcnB*, encoding poly(A) polymerase I (PAP I) responsible for RNA polyadenylation and degradation, upregulates the proton-consuming GAD system and improves membrane properties, redox state, and energy level. Based on *pcnB* repression, further repression of *acrD* enhances FFAs efflux and increases FFAs production. The engineered *pcnB*^{i}-*acrD*^{i}-*fadR*$^{+}$ strain achieves the highest titer of FFAs in *E. coli* reported to date. This study demonstrates the genome-scale screen of genetic determinants that confer improved microbial physiology for FFAs overproduction.

Results

Genome-scale CRISPRi screen identifies *pcnB* repression enabling FFAs overproduction

To identify genetic determinants conferring physiological benefits for FFAs overproduction, we conducted a genome-scale CRISPRi screen combining fluorescence-activated cell sorting (FACS) and next-generation sequencing (NGS) (Fig. 1a). The detailed screening procedure is outlined in the "Methods" section. Briefly, a previously published plasmid library containing 55,671 sgRNAs[20] was transformed into *E. coli* strain CF (an MG1655 (DE3) derivative with *fadE* deletion) carrying the pCF plasmid for expression of dCas9 and the truncated fatty acyl-ACP thioesterase TesA′. After cultivation for 40 h after IPTG induction, the cell library before sorting (BS) was collected and stained with the lipophilic dye Nile Red, which exhibited a strong positive correlation between fluorescence intensity and FFAs titer quantified by gas chromatography-mass spectrometry (GC-MS)[21,22]. For reliable screening of such a large and diverse population, the top 1% of cells with the highest fluorescence intensity were considered potential FFAs-overproducers and isolated as the cell library after sorting (AS). Subsequently, NGS was conducted to profile the cell libraries BS and AS, allowing us to track variations in sgRNA distribution (Fig. 1b). Genetic perturbations conferring better physiology would achieve a higher proportion within the library after cultivation and exhibit higher sequencing reads detected through NGS within the sorted cells. Consequently, the top 30 sgRNAs with the highest reads in AS, representing genotypes with high proportions in the sorted cell population, were chosen as potential genetic candidates conferring physiological advantages for FFAs overproduction (Fig. 1c). Additionally, sgRNA fitness, commonly used in screening essential, auxotrophic, and chemical tolerance-related genes[20,23], was also calculated to analyze the change in relative abundance of sgRNA in AS compared to BS. Thus, the top 30 sgRNAs with the highest fitness values were also chosen as candidates for screening FFAs overproducers (Fig. 1 d).

To verify the efficacy of the selected candidates in FFAs production, corresponding strains were constructed and applied for reverse engineering (Fig. 1a). The CF strain, which did not undergo any genome modulation, produced 747 mg L^{-1} FFAs (Fig. 1e). In comparison, nine engineered strains (namely *gyrA*_9, *pcnB*_27, *pcnB*_591, *pcnB*_829, *ygcU*_1142, *pcnB*_956, *pcnB*_1214, *pcnB*_1339, and *hemX*_50) exhibited FFAs titers over 50% higher than the CF strain, along with enhanced cell growth (Fig. 1e and Supplementary Fig. 1). Particularly noteworthy is that six of these strains expressed sgRNAs specifically targeting the *pcnB* gene with varying levels of repression efficiency (Fig. 1e and Supplementary Fig. 2). Among them, the *pcnB*_956 strain with *pcnB* repressed to 12% of the CF strain demonstrated the highest FFAs production of 2916 mg L^{-1}, which was 3.9-fold that of the CF strain (Fig. 1e and Supplementary Fig. 2). These results underscore the significant role of *pcnB* repression in driving FFAs overproduction.

To confirm whether the increased FFAs production in the *pcnB*_956 strain resulted from *pcnB* repression, we determined the transcript level of *pcnB* throughout the cultivation process and assessed the impact of repressing the *pcnB-folk* operon. Firstly, we employed RT-qPCR analysis and observed that the *pcnB* mRNA level in the *pcnB*_956 strain was reduced to 27%, 51%, 13%, 44%, and 55% of that in the CF strain at 3, 9, 12, 24, and 40 h of IPTG induction, respectively, confirming the effective repression of *pcnB* expression through CRISPRi (Fig. 1f). Secondly, we targeted the *folK* gene within the *pcnB-folk* operon for specific repression. Given that *pcnB* is situated upstream of this polycistronic operon, *pcnB* repression by CRISPRi might exert a polar effect and suppress the expression of its downstream gene[24], *folK*. Thus, there was a possibility that the increased FFAs production in the *pcnB*_956 strain could be attributed to the suppression of *folk*. Nevertheless, FFA assay results demonstrated that inhibiting *folK* alone did not increase FFAs titer (Fig. 1g), ruling out the influence of the polar effect within the *pcnB-folk* operon for FFAs overproduction. Additionally, we also constructed the *pcnB* deletion strain (Δ*pcnB*) and *pcnB* mutation strains (E108A and N138H) with decreased activity relative to the wild type[25]. The corresponding derivative strains (*pcnB*$^{-}$, *pcnB*^{mE}, and *pcnB*^{mN}) carrying the pCF plasmid were applied for FFAs production. As a result, the *pcnB*$^{-}$ strain slightly increased FFAs titer to 1010 mg L^{-1} compared to the CF strain, whereas the *pcnB*^{mE} and *pcnB*^{mN} strains produced 3140 mg L^{-1} and 3274 mg L^{-1} FFAs, 420% and 438% of that of the CF strain, respectively (Supplementary Fig. 3). These results indicate that *pcnB* deletion has a limited effect on enhancing FFAs production, while reduced *pcnB* function significantly increases FFAs titer whether by CRISPRi or mutants.

To reduce the metabolic burden of maintaining multiple plasmids, we integrated the expression of TesA′, dCas9, and *pcnB*_956 sgRNA into a single plasmid. The DNA sequence for expressing *pcnB*_956 sgRNA was transferred from the pSg-*pcnB*_956 plasmid to the pCF plasmid, resulting in the pCF-*pcnB*^{i} plasmid. The strain MG carrying the pCF-*pcnB*^{i} plasmid, designated as the *pcnB*^{i} strain, showed a slight increase in cell growth and FFAs titer (2992 mg L^{-1}) compared to the *pcnB*_956 strain, and a higher growth rate and OD_{600} value than the CF strain (Fig. 1h and Supplementary Fig. 4). Thus, the *pcnB*^{i} strain was applied for subsequent analyses.

https://doi.org/10.1038/s41467-025-58368-3

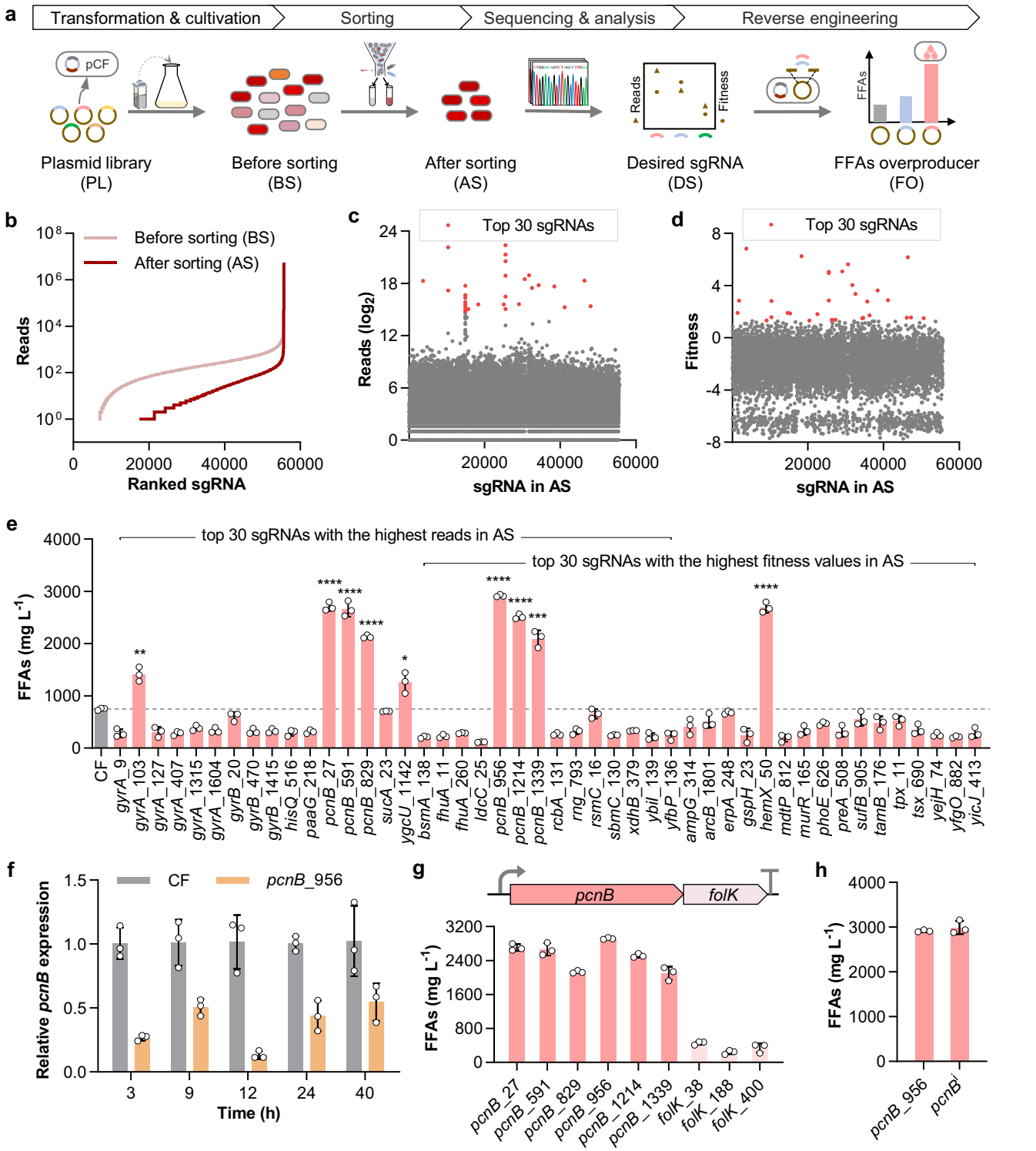

Fig. 1 | Genome-scale CRISPRi screen identifies *pcnB* repression enabling FFAs overproduction in *E. coli*. **a** Schematic illustration of genome-scale CRISPRi screen and reverse engineering for FFAs overproduction. **b** sgRNAs are enriched in the library after sorting (AS) compared to before sorting (BS). sgRNAs are ranked by their reads from low to high. **c** Top 30 sgRNAs with the highest reads in AS are applied in subsequent reverse engineering. sgRNAs are ranked alphabetically by their names. **d** Top 30 sgRNAs with the highest fitness values in AS are applied in subsequent reverse engineering. sgRNAs are ranked alphabetically by their names. Fitness is defined as the change in normalized reads of the sgRNA in AS relative to BS, where normalized reads are calculated by dividing the sgRNA reads plus one by the total reads. **e** *pcnB* repression significantly enhances FFAs production. The dashed line denotes the FFAs titer of the CF strain. The *pcnB*_956 strain achieved the highest FFAs titer and was applied for the subsequent analyses. The *P*-value is calculated with an unpaired two-tailed *t*-test; $^{*}P = 0.0117$, $^{**}P = 0.0011$, $^{***}P = 0.0001$, and $^{****}P < 0.0001$ comparing the engineered strain vs. CF. **f** Relative mRNA level of *pcnB* is downregulated in the *pcnB*_956 strain compared to the CF strain. Samples were collected at 3, 9, 12, 24, and 40 h after IPTG induction for RT-qPCR assay. **g** Increase in FFAs production is attributed to *pcnB* repression rather than *folK* repression. The *folk* gene is located downstream of the *pcnB-folK* operon. **h** *pcnB* repression using one plasmid (the $pcnB^{i}$ strain) obtains comparable FFAs production as using two plasmids (the *pcnB*_956 strain). Data are presented as mean ± SD ($n = 3$ biological replicates). Source data are provided as a Source Data file.

Collectively, these findings highlight that the substantial improvement in FFAs production is attributable to the specific repression of *pcnB*. Therefore, our genome-scale CRISPRi screen identified an extraordinary gene target, *pcnB*, previously unassociated with FFAs production.

pcnB repression enhances the stability and abundance of the *gadAXE* transcripts

Here we report that *pcnB* repression facilitates FFAs overproduction, with the underlying mechanisms previously undefined. The *pcnB* gene encodes poly(A) polymerase I (PAP I), the primary PAP responsible for RNA polyadenylation at the 3′ end in *E. coli*[26], which provides a toe-hold for 3′-5′ exonucleases and assists in the degradation of polyadenylated RNAs[27,28] (Fig. 2a). When *pcnB* expression is repressed, polyadenylation-mediated degradation is expected to be reduced, resulting in increased stability and abundance of the targeted RNAs (Fig. 2a). Previous studies have indicated that the majority of mRNAs undergo some degree of polyadenylation[28,29]. It is pivotal to identify which RNAs are stabilized and accumulated due to reduced polyadenylation through *pcnB* repression, thereby contributing to FFAs overproduction in the *pcnB*^{i} strain. Consequently, we conducted comparative transcriptomic and proteomic analyses between the engineered strain *pcnB*^{i} and the control strain CF. Differential expression analysis revealed significant changes in the expression of hundreds of genes between *pcnB*^{i} and CF strains (Supplementary Fig. 5), indicating widespread regulation of cellular processes resulting from *pcnB* repression.

We conducted the KEGG enrichment analysis of the differentially expressed genes in the *pcnB*^{i} strain compared to the CF strain. The upregulated genes were significantly enriched in five pathways at the transcript level and seven at the protein level (Supplementary Fig. 6). Although the downregulated genes displayed significant enrichment in five pathways at the protein level, no pathway was significantly enriched at the transcript level (Supplementary Fig. 7). Given that *pcnB* repression enhances RNA stability and abundance, we focused on the enriched pathways of the upregulated genes to identify potential targets for FFAs overproduction. Notably, alanine, aspartate, and glutamate metabolism was significantly enriched at both the transcript and protein levels (Supplementary Fig. 6). Within this pathway, *gadA*, *gadB*, *glmS*, and *glsA* exhibited substantial upregulation in *pcnB*^{i} compared to CF, with fold changes of 5.9, 4.8, 2.7, and 2.2 at the transcript level, and 8.8, 10.5, 3.9, and 3.5 at the protein level, respectively (Fig. 2b). Additionally, *gadX* and *gadE* (encoding transcriptional activators of the operons of *gadA*, *gadB*, and *glsA*)[30,31] and *gadC* (encoding a membrane transporter) were also upregulated in *pcnB*^{i} compared to CF (Fig. 2b, c). Among the above seven genes, it has been reported that the *glmS* transcript is not modified by PAP I but is activated by a small RNA that can be polyadenylated[32]. However, for the other six genes (*gadA*, *gadB*, *glsA*, *gadX*, *gadE*, and *gadC*), it remains unclear whether the accumulation of their transcripts in the *pcnB*^{i} strain is due to reduced polyadenylation.

To investigate whether the *gadA*, *gadB*, *glsA*, *gadX*, *gadE*, and *gadC* RNAs were regulated by PAP I-mediated polyadenylation, we assessed the stability of these specific RNAs through rifampicin treatment coupled with RT-qPCR analysis. The *osmY* and *dxs* RNAs were also assayed and served as positive and negative controls, as they have been confirmed in previous studies to be and not to be polyadenylated by PAP I, respectively[33]. Four strains were utilized here, including CF, *pcnB*^{i} (*pcnB* repression), *pcnB*$^{+}$ (*pcnB* overexpression), and *pcnB*$^{-}$ (*pcnB* deletion). We found that all tested RNAs in the *pcnB*$^{+}$ strain were almost degraded within two minutes (Fig. 2d, e), consistent with previous studies that PAP I overproduction significantly increased the number of polyadenylated transcripts and accelerated their degradation[28,29]. In the CF, *pcnB*^{i}, and *pcnB*$^{-}$ strains, the stability of the tested RNAs presented two patterns (Fig. 2d, e). The degradation curves for *gadB*, *gadC*, *glsA*, and *dxs* (negative control) RNAs showed substantial overlap across the CF, *pcnB*^{i}, and *pcnB*$^{-}$ strains (Fig. 2d), indicating almost no significant difference in their stability by *pcnB* modulation (Supplementary Fig. 8). Conversely, for the *gadA*, *gadX*, *gadE*, and *osmY* (positive control) RNAs, the degradation rates were notably reduced in the *pcnB*^{i} and *pcnB*$^{-}$ strains compared to the CF strain (Fig. 2e), suggesting enhanced stability when *pcnB* function was compromised (Supplementary Fig. 8). Therefore, it is likely that the *gadA*, *gadX*, and *gadE* RNAs are regulated by PAP I-mediated polyadenylation.

We then conducted the 3′-RACE assay for *gadAX*, *gadE*, and control RNAs (*osmY* as positive and *dxs* as negative). Complementary DNA (cDNA) was synthesized from total RNA of the CF, *pcnB*^{i}, *pcnB*$^{+}$, and *pcnB*$^{-}$ strains using the oligo(dT)-containing adapter primer (AP) and served as the template for PCR amplification with gene-specific forward primers and an abridged universal amplification primer (AUAP)[34] (Fig. 2f). Agarose gel electrophoresis images displayed specific DNA bands from PCR products amplified using *gadX*, *gadE*, and *osmY* (positive control) forward primers, whereas no bands were observed with the *dxs* (negative control) forward primer (Fig. 2f). This result indicates the presence of poly(A) at the 3′ end of *gadAX* and *gadE* transcripts, suggesting PAP I-mediated polyadenylation of these RNAs. We also found that DNA bands were faint from CF and *pcnB*$^{+}$, but were distinct from *pcnB*^{i} and *pcnB*$^{-}$ (Fig. 2f). The possible reason was that the reduced polyadenylation led to the increased abundance of targeted RNA, providing more templates for cDNA synthesis and subsequent PCR amplification. These results support that *gadAX* and *gadE* RNAs are regulated by PAP I-mediated polyadenylation.

We have demonstrated that the stability and abundance of the *gadAX* and *gadE* RNAs are enhanced upon *pcnB* repression. As activators, GadX and GadE can upregulate the expression of genes in the GAD system (*gadAXEBC*)[30,31]. We thus determined the expression of these GAD genes by RT-qPCR where *pcnB* expression was non-regulated (CF), repressed (*pcnB*^{i}), or deprived (*pcnB*$^{-}$). The result showed that *gadAXEBC* were all upregulated more than 4.8-fold in the *pcnB*^{i} or *pcnB*$^{-}$ strains compared to the CF strain (Fig. 2g). Additionally, it is noteworthy that FFAs production can exert an increase in intracellular proton level and the GAD genes are known to be involved in proton consumption[35,36]. Thus, the observed upregulation of GAD genes in the *pcnB*^{i} strain might be attributed to FFAs overproduction rather than *pcnB* repression. To clarify the causal relationship, the transcript levels of the GAD genes were also examined in strains absent *tesA*′ expression and without FFAs overproduction (denoted as CF^{-}, *pcnB*^{i}F^{-}, and *pcnB*$^{-}$F^{-} strains, respectively, Supplementary Fig. 9). RT-qPCR results revealed that the transcripts of GAD genes in the *pcnB*^{i}F^{-} and *pcnB*$^{-}$F^{-} strains were more than 5.0-fold of those in the CF^{-} strain, similar to the patterns observed in FFAs-producing strains expressing *tesA*′ (Fig. 2g). A slight discrepancy in relative expression in *pcnB*^{i} vs. *pcnB*^{i}F^{-} and *pcnB*$^{-}$ vs. *pcnB*$^{-}$F^{-} might be due to TesA′ overexpression or not, which leads to differences in transcription, translation, and metabolism[37,38]. Notably, relative expression of the GAD genes was significantly increased upon *pcnB* repression or deletion both in the context of FFAs overproduction and without FFAs overproduction, confirming that *pcnB* repression leads to the upregulation of GAD genes.

pcnB repression alleviates proton-induced cellular damage and improves microbial physiology

The accumulated FFAs (HA) in the neutral cytoplasm could dissociate into anions (A^-) and protons (H^+), leading to an increase in intracellular protons (H^+) level[36,39]. The accumulation of intracellular protons (H^+) is implicated in cellular damage, including (i) membrane damage, (ii) redox stress, and (iii) energy deprivation[40–42] (Fig. 3a). As we demonstrated above, *pcnB* repression upregulates the expression of genes in the GAD system (Fig. 2). Intriguingly, the GAD system is involved in proton consumption and is also known as the glutamate-dependent

https://doi.org/10.1038/s41467-025-58368-3

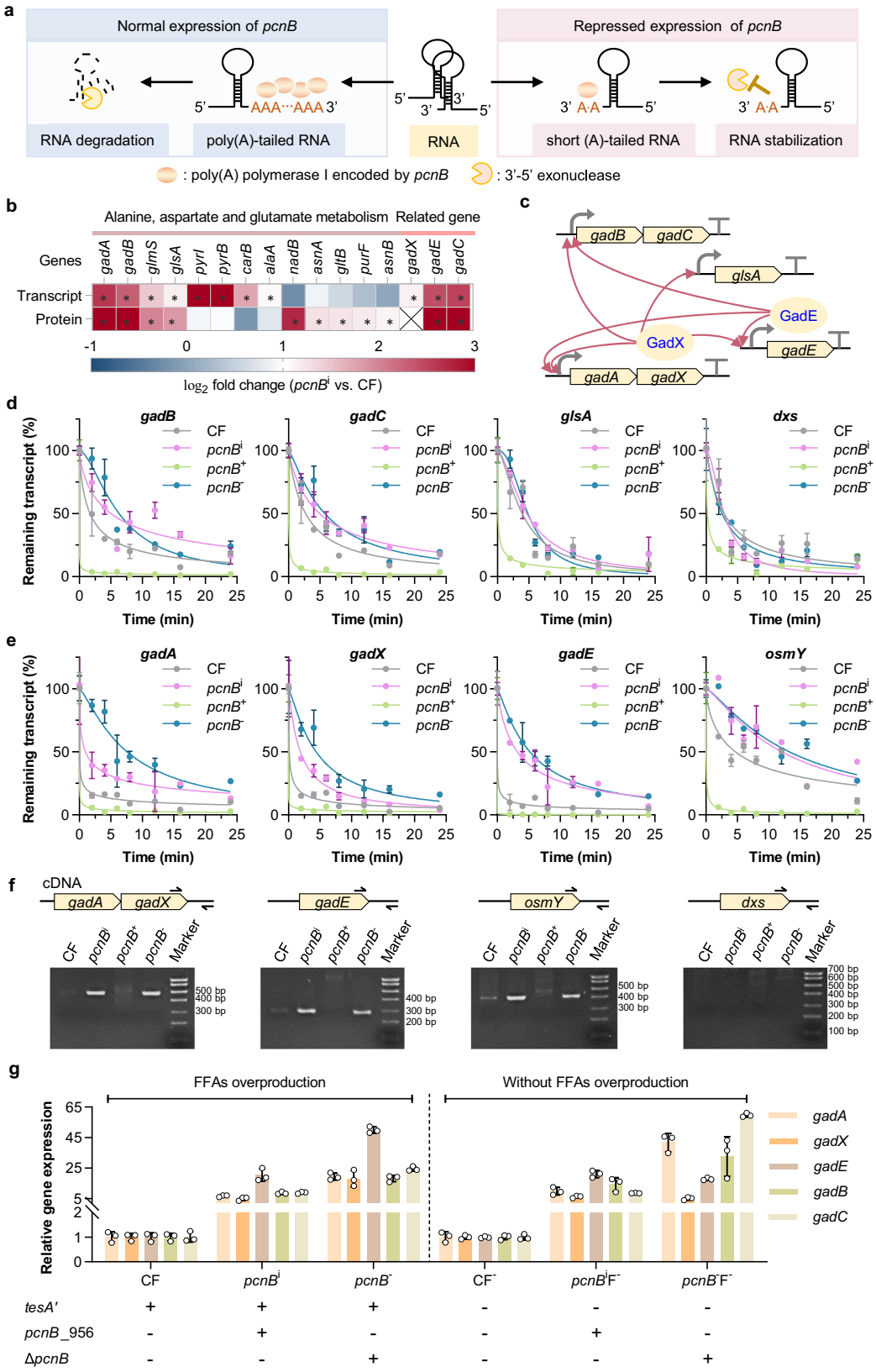

acid resistance system (AR2), considered the most efficient AR system in *E. coli*[40,41]. Specifically, GlsA catalyzes the conversion of glutamine to glutamate and ammonia, neutralizing protons around the cells. Subsequently, GadA and GadB convert glutamate into γ-aminobutyric acid (GABA) and carbon dioxide, accompanied by intracellular proton consumption (Fig. 3a). Thus, we hypothesized that *pcnB* repression could alleviate proton-induced cellular damage, thereby improving microbial physiology and boosting FFAs biosynthesis in the *pcnB*^{i} strain.

To validate our hypothesis, we assessed the cellular physiology of the CF and *pcnB*^{i} strains from three aspects: (i) membrane properties, (ii) redox state, and (iii) energy level. Firstly, in terms of membrane

Fig. 2 | *pcnB* repression enhances the stability and abundance of the *gadAXE* transcripts by reducing RNA polyadenylation. a Schematic illustration of RNA polyadenylation at the 3′ end by PAP I (encoded by *pcnB*) and subsequent degradation by 3′-5′ exonucleases. **b** *pcnB* repression significantly upregulates the expression of genes involved in the alanine, aspartate, and glutamate metabolism. Gene expression data was from comparative transcriptomic and proteomic analyses of the $pcnB^{i}$ and CF strains. The asterisk indicates the gene with $\log_2$ fold change >1 and *q*-value < 0.05 (at the transcript level) or *p*-value < 0.05 (at the protein level). **c** Schematic illustration of the *gadAX*, *gadE*, *gadBC*, *glsA-ybaT* operons and their transcriptional activators GadX and GadE. **d** Degradation curves for the *gadB*, *gadC*, *glsA*, or *dxs* RNAs almost overlap among the CF, $pcnB^{i}$, and $pcnB^{-}$ strains. The *dxs* RNA is the negative control. **e** Degradation rate of the *gadA*, *gadX*, *gadE*, and *osmY* RNAs is reduced in the $pcnB^{i}$ (with *pcnB* repressed) or $pcnB^{-}$ (with *pcnB* deleted) strain compared to the CF strain. The *osmY* RNA is the positive control. Cells at 12 h after IPTG induction were treated with rifampicin to inhibit transcription and then sampled for RT-qPCR assay (**d**, **e**). **f** Agarose gel electrophoresis images of the 3′-RACE assay display specific DNA bands amplified using *gadX*, *gadE*, and *osmY* forward primers, indicating PAP I-mediated polyadenylation of these RNAs. The arrow represents the position of the primer used. These experiments were repeated three times with similar results. **g** Relative mRNA levels of the *gadAXEBC* transcripts are upregulated when *pcnB* expression is repressed or deleted, both in the presence (expressing *tesA′* that encodes the truncated fatty acyl-ACP thioesterase) and absence (not expressing *tesA′*) of FFAs overproduction. Samples were collected at 3 h after IPTG induction for RT-qPCR assay. Data are presented as mean ± SD ($n = 3$ biological replicates). Source data are provided as a Source Data file.

properties, we evaluated membrane integrity and cell surface hydrophobicity. Membrane integrity was determined by propidium iodide (PI) staining and flow cytometry, revealing an increase in the proportion of intact cells (PI-negative) from 58.0% in the CF strain to 88.0% in the $pcnB^{i}$ strain (Fig. 3b). Cell surface hydrophobicity, measured using the microbial adhesion to hydrocarbon (MATH) method, decreased from 21.2% in the CF strain to 15.8% in the $pcnB^{i}$ strain (Fig. 3c). It is reported that increased membrane integrity correlates with reinforced cellular viability[8], and reduced cell surface hydrophobicity could mitigate the intercalation of hydrophobic compounds into the membrane[43]. Thus, *pcnB* repression enhances membrane properties, supporting improved cellular physiologies for FFAs overproduction.

Secondly, for redox state assessment, we analyzed ROS levels in the CF and $pcnB^{i}$ strains. As measured by a microplate reader, ROS level in the $pcnB^{i}$ strain decreased by 88.0% compared to the CF strain (Fig. 3d). This reduction was consistently observed in microscope images, where stronger green fluorescent foci filled a large percent of the CF cells and almost no fluorescent foci were visible in the $pcnB^{i}$ cells (Fig. 3d). These results suggest a significant reduction of intracellular ROS due to *pcnB* repression, benefiting cellular redox homeostasis.

Thirdly, ATP levels in the CF and $pcnB^{i}$ strains were measured to assess the impact of *pcnB* repression on energy levels. As a result, the ATP level in the $pcnB^{i}$ strain increased by 52% compared to the CF strain after induction of *pcnB* repression for 12 h, and this increase further amplified to 111% compared to the CF strain after induction of *pcnB* repression for 24 h (Fig. 3e). Notably, RNA polyadenylation by PAP I is also an ATP-consuming process[26]. Therefore, the repression of *pcnB* is suspected to reduce polyadenylation and conserve more energy for FFAs production.

Additionally, we also detected fermentation byproducts (pyruvate, succinate, lactate, formate, and acetate) of the CF and $pcnB^{i}$ strains. As a result, no detectable amount of pyruvate, succinate, lactate, or formate was detected, while acetate was found accumulated in the fermentation media. Specifically, the CF and $pcnB^{i}$ strains accumulated 476 and 328 mg L^{-1} acetate, respectively (Supplementary Fig. 10). Nevertheless, the slight decrease in the byproduct acetate (148 mg L^{-1}) observed in the $pcnB^{i}$ strain compared to the CF strain is insufficient for the substantial increase in FFAs production from 747 mg L^{-1} in the CF strain to 2992 mg L^{-1} in the $pcnB^{i}$ strain (Fig. 1).

Given that *pcnB* repression confers improved microbial physiologies, FFAs overproduction may be a general outcome of *pcnB* repression in multiple contexts. We thus utilized diversified *E. coli* strains or different substrates for fermentation and FFAs assay. As a result, *pcnB* repression contributed to an increase of FFAs titer by 300%, 53%, 149%, 199%, and 264% in MG1655(DE3) Δ*fadE*, JM109(DE3), AD494(DE3), BL21-trxB(DE3), and origami(DE3), respectively (Fig. 4 and Supplementary Fig. 11). When using glucose as substrate, FFAs titer also increased by 284% and 180% upon *pcnB* repression in MG1655(DE3) Δ*fadE* and JM109(DE3), respectively (Fig. 4 and Supplementary Fig. 11). These results highlight the universality of *pcnB* repression in boosting FFAs biosynthesis.

Iterative CRISPRi screen identifies *acrD* repression further enhancing FFAs production

To further enhance FFAs production, we attempted combinatorial perturbation by targeting *pcnB* along with other beneficial genetic determinants identified through our initial genome-scale CRISPRi screen (Fig. 1e). However, such a program did not yield the anticipated improvement in FFAs production (Supplementary Fig. 12). Previous studies have suggested that the optimal synergism does not necessarily arise from the combinations of beneficial genetic determinants when tested individually[44,45]. Therefore, we were inspired to conduct a second round of genome-scale CRISPRi screening based on *pcnB* repression to investigate optimal combinations that could further enhance FFAs production. The experimental procedures and data processing workflow were similar to those used in the first round of screening. NGS analysis revealed a significant reduction in sgRNA distribution in the cell library after sorting (AS) compared to before sorting (BS) (Fig. 5a), demonstrating the reliability and effectiveness of the screen conducted in this round.

To verify the optimal combinatorial perturbation for enhancing FFAs production, we selected the top 30 sgRNAs with the highest reads and the top 30 sgRNAs with the highest fitness values for reverse engineering (Fig. 5b, c). Plasmids harboring the corresponding sgRNAs were constructed and individually introduced into the $pcnB^{i}$ strain. The results of FFA assay showed that the $pcnB^{i}$-*acrD*_2252 strain achieved the highest FFAs production of 3974 mg L^{-1}, which was 1.3-fold and 5.3-fold of the $pcnB^{i}$ and CF strains, respectively (Fig. 5d and Supplementary Fig. 13a). RT-qPCR analysis confirmed effective suppression of *pcnB* and *acrD* expression in the $pcnB^{i}$-*acrD*_2252 strain, with mRNA levels reduced to 17% and 28% of those in the CF strain, respectively (Fig. 5e). Moreover, the expression of sgRNAs targeting other regions of the *acrD* open reading frame in the $pcnB^{i}$ strain also endowed an increase in FFAs production ranging from 14% to 22% (Fig. 5f and Supplementary Fig. 13b). Additionally, we engineered a single plasmid for simultaneous repression of *pcnB* and *acrD*, constructing the $pcnB^{i}$-$acrD^{i}$ strain, which showed a slight increase in cell growth and FFAs titer (4120 mg L^{-1}) compared to the $pcnB^{i}$-*acrD*_2252 strain (Fig. 5g and Supplementary Fig. 13c). Overall, these results demonstrate that combinatorial repression of *pcnB* and *acrD* can significantly enhance FFAs production.

acrD repression increases FFAs production by enhancing efflux based on synergistic repression of *pcnB*

AcrD and AcrB function as efflux transporters that require interaction with outer membrane channel TolC and periplasmic lipoprotein AcrA, wherein AcrD primarily pumps hydrophilic substrates and AcrB prefers efflux of lipophilic compounds[46,47]. Reduced AcrD level potentially frees up more available TolC and AcrA for interaction with AcrB, thereby enhancing the efflux of lipophilic FFAs (Fig. 6a). This is

https://doi.org/10.1038/s41467-025-58368-3

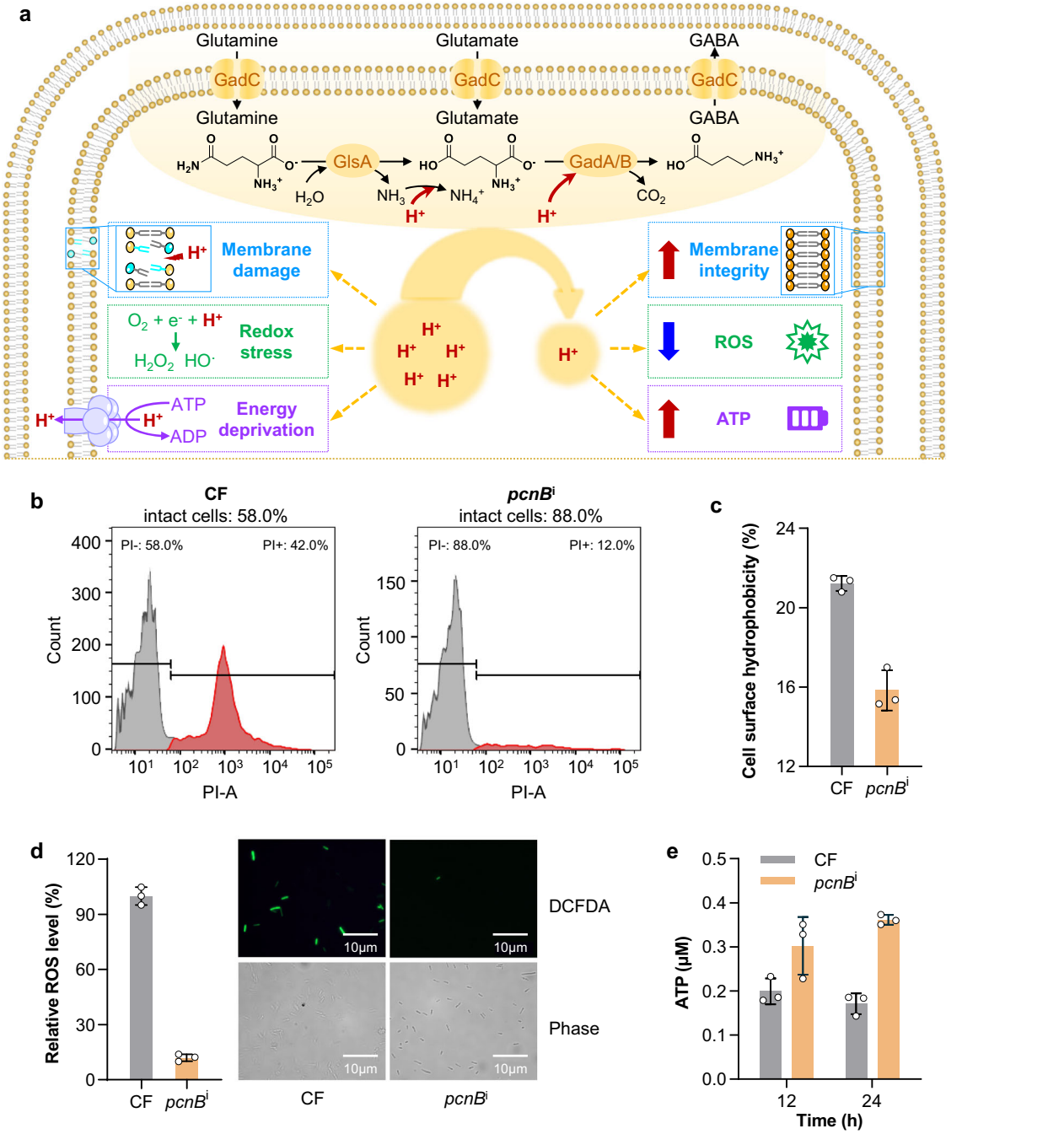

Fig. 3 | *pcnB* repression alleviates proton-induced cellular damage and improves microbial physiology. a Schematic illustration depicting the GAD system consuming intracellular proton and thereby alleviating membrane damage, redox stress, and energy deprivation. ROS, Reactive oxygen species. **b**, **c** *pcnB* repression increases membrane integrity (**b**) and reduces cell surface hydrophobicity (**c**). Samples were collected after 12 h of IPTG induction. Membrane integrity was detected by propidium iodide (PI) staining and flow cytometry, represented by the percentage of intact cells. Cell surface hydrophobicity was determined by the MATH method. **d** Intracellular ROS level is reduced by *pcnB* repression. Samples were collected after 12 h of IPTG induction, and fluorescence was measured using the corresponding Assay Kit and a microplate reader (left) or a microscope (right). DCFDA, 2,7-Dichlorofluorescein diacetate. **e** *pcnB* repression benefits cellular ATP level. Samples were collected after 12 and 24 h of IPTG induction and detected by the corresponding Assay Kit. These experiments in (**b**, **d**) were repeated three times with similar results. Data are presented as mean ± SD ($n = 3$ biological replicates). Source data are provided as a Source Data file.

evidenced by the increased proportion of extracellular FFAs from 34% and 49% in the CF and *pcnB*^{i} strains to 66% and 80% in the *acrD*^{i} and *pcnB*^{i}-*acrD*^{i} strains, respectively (Fig. 6b). However, although *acrD* repression further increased FFAs titer on the basis of *pcnB* repression, *acrD* repression alone (*acrD*^{i}) even decreased FFAs production and cell growth compared to the CF strain (Fig. 6c and Supplementary Fig. 13d). Given that *acrD* encodes a membrane protein, its repression likely disturbs membrane homeostasis. As shown in the scanning electron microscope (SEM) images, the *acrD*^{i} cells appeared shriveled, collapsed, severely deformed, and even fragmented (Fig. 6d). In contrast, the *pcnB*^{i}-*acrD*^{i} cells exhibited uniform structures with intact shapes and smooth surfaces, representing a marked improvement compared to the CF and *acrD*^{i} cells (Fig. 6d). This improvement in cellular integrity is further supported by PI staining and flow cytometry analysis (Fig. 6e). Only 19.5% of *acrD*^{i} cells maintained intact membranes, significantly lower than the 58.0% observed in CF cells. Notably, 71.0%

https://doi.org/10.1038/s41467-025-58368-3

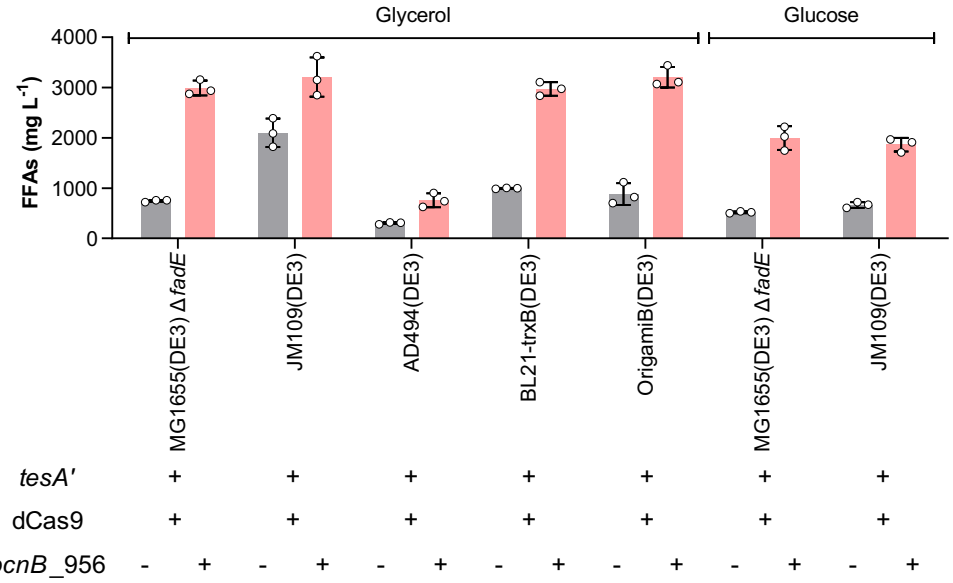

Fig. 4 | The improvement in FFAs production by *pcnB* repression is universal in multiple contexts. *pcnB* repression via expressing the dCas9 protein and the *pcnB*_956 sgRNA enhanced FFAs production in the JM109(DE3), AD494(DE3), BL21-trxB(DE3), and OrigamiB(DE3) strains using glycerol as substrate, resembling that in the MG1655(DE3) Δ*fadE* strain. Using glucose as substrate, *pcnB* repression also enhanced FFAs production in the MG1655(DE3) Δ*fadE* and JM109(DE3) strains. The *tesA′* gene encodes the truncated fatty acyl-ACP thioesterase. Data are presented as mean ± SD ($n = 3$ biological replicates). Source data are provided as a Source Data file.

of *pcnB*^{i}-*acrD*^{i} cells maintained intact membranes, which represents a significant improvement over the *acrD*^{i} and even CF strains (Fig. 6e). These data indicate that the repression of *pcnB* substantially mitigates the membrane damage caused by *acrD* downregulation.

Overall, the improvement in FFAs production by inhibiting *acrD* is achieved only in conjunction with *pcnB* repression (Fig. 6c). This intriguing phenomenon can be explained by two factors: intracellular FFAs level and cell membrane state. When *pcnB* and *acrD* were simultaneously inhibited, *pcnB* repression elevates the FFAs pool to a certain threshold, allowing FFAs efflux induced by *acrD* repression to alleviate intracellular stress and robustly drive FFAs biosynthesis. Moreover, *pcnB* repression enhances membrane properties, helping to mitigate membrane damage caused by *acrD* repression, thus maintaining the *pcnB*^{i}-*acrD*^{i} strain in an improved physiological state for FFAs overproduction. In contrast, a low FFAs titer (inhibiting *acrD* alone) does not require enhanced efflux, and such disturbance instead causes damage to the cell membrane, which is detrimental to microbial biosynthesis. Our results provide insights into the functional realization and remediation achieved through the synergistic regulation of dual genetic determinants.

FFAs production by fed-batch fermentation

To further enhance FFAs biosynthesis, the transcriptional activator of fatty acid biosynthetic genes (FadR) was overexpressed in the *pcnB*^{i}-*acrD*^{i} strain. The results showed that the strain with *fadR* controlled by the P_{BAD} promoter (*pcnB*^{i}-*acrD*^{i}-*fadR*$^{+}$) produced 5105 mg L^{-1} FFAs (Fig. 7a and Supplementary Fig. 14a), which was applied for fed-batch fermentation. After cultivation for 41.7 h, the *pcnB*^{i}-*acrD*^{i}-*fadR*$^{+}$ strain achieved a remarkable FFAs production of 35.1 g L^{-1}, with a productivity of 0.84 g L^{-1} h^{-1} and a yield of 0.20 g g^{-1} glycerol (Fig. 7b). This high titer resulted in visible FFAs at the top of the culture medium after centrifugation (Supplementary Fig. 14b). Additionally, dead cells or fatty acid particles were stuck on the fermenter inner wall during the cultivation process[22,48] (Supplementary Fig. 14c), contributing to an extra amount of FFAs that is difficult to precisely quantify and not included in the reported titer. To the best of our knowledge, this study achieved the maximum FFAs titer in *E. coli* and the highest productivity of FFAs production through microbial fermentation reported to date[19,48].

Discussion

Physiology-oriented engineering plays a pivotal role in improving the biosynthesis of desired products due to its intrinsic and profound effects on microbial metabolisms; however, the complexity of physiological architecture severely hinders engineering cell factories for chemical overproduction. In our work, we leveraged a CRISPRi library combining FACS and NGS to systematically identify genetic determinants that confer physiological advantages for FFAs overproduction. This genome-scale modulation and high-through screen not only allowed us to map the potential determinants within the microbial genome for FFAs production but also to integrate genetic insights with physiological functionalities.

One of the key successes of our study was identifying that *pcnB* repression confers physiological benefits for FFAs overproduction. Recent studies have also associated *pcnB* repression with improved microbial phenotypes. For example, tolerance toward furfural and isobutanol was enhanced upon knockdown of *pcnB* in *E. coli*[20], and L-lactate productivity was increased via *pcnB* repression in *Synechocystis* sp PCC 6803[23]. These findings underscore the substantial potential of *pcnB* for engineering biotechnological traits of interest. However, how *pcnB* repression modulates genetic networks to adapt to such enhanced microbial phenotypes remains unclear, impeding a deeper understanding of the metabolic connections and the full exploitation of cellular capabilities. Here we demonstrated how *pcnB* repression confers FFAs overproduction through systematic analyses of the regulation of gene expression and cell function (Supplementary Fig. 15). Regarding regulation of gene expression, we verified that *pcnB* repression increases the stability and abundance of the *gadAXE* transcripts by reducing polyadenylation; GadX and GadE, transcriptional activators of the GAD system[30,31], subsequently upregulate the expression of GAD genes (Fig. 2). Regarding regulation of cell function, the GAD system is involved in proton consumption and recognized as the most efficient acid resistance system in *E. coli*, mitigating proton-induced cellular damage[40,41]; We determined that *pcnB* repression improved membrane integrity, decreased ROS level, and increased ATP level, thereby endowing improved cellular physiology to support FFAs overproduction (Fig. 3). Our findings provide valuable insights into microbial engineering for enhanced chemical tolerance and biosynthetic efficiency.

https://doi.org/10.1038/s41467-025-58368-3

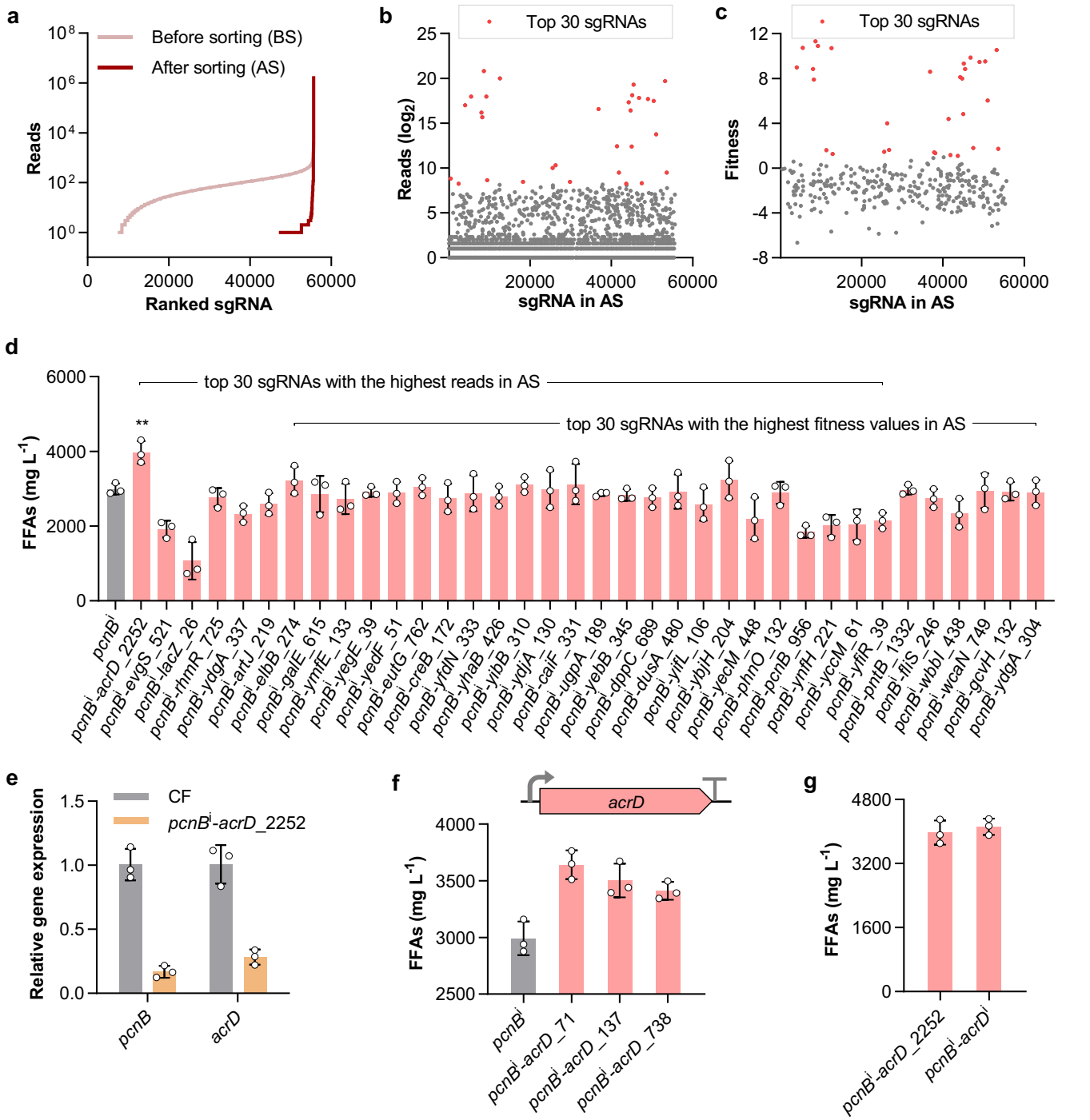

Fig. 5 | Iterative CRISPRi screen identifies *acrD* repression further enhancing FFAs production on the basis of *pcnB* repression. a sgRNAs are enriched in the library after sorting (AS) compared to before sorting (BS) in the second round of the CRISPRi screen. sgRNAs are ranked by their reads from low to high. **b** Top 30 sgRNAs with the highest reads in AS are applied in subsequent reverse engineering. sgRNAs are ranked alphabetically by their names. **c** Top 30 sgRNAs with the highest fitness values in AS are applied in subsequent reverse engineering. sgRNAs are ranked alphabetically by their names. Fitness is defined as the change in normalized reads of the sgRNA in AS relative to BS, where normalized reads are calculated by dividing the sgRNA reads plus one by the total reads. **d** *acrD* repression through the *acrD*_2252 sgRNA further enhances FFAs production based on *pcnB*^{i}. The *P*-value is calculated with an unpaired two-tailed *t*-test; $^{**}P = 0.0072$ comparing *pcnB*^{i}-*acrD*_2252 vs. *pcnB*^{i}. **e** Relative mRNA levels of *pcnB* and *acrD* are downregulated in the *pcnB*^{i}-*acrD*_2252 strain compared to the CF strain. Samples were collected at 3 h after IPTG induction for RT-qPCR assay. **f** Expression of other sgRNAs targeting *acrD* also enhances FFAs production on the basis of *pcnB*^{i}. **g** Repression of *acrD* and *pcnB* using one plasmid (the *pcnB*^{i}-*acrD*^{i} strain) obtains comparable FFAs production as using two plasmids (the *pcnB*^{i}-*acrD*_2252 strain). Data are presented as mean ± SD ($n = 3$ biological replicates). Source data are provided as a Source Data file.

FFAs production in *E. coli* has been systematically studied and progressively enhanced over the past years. Strategies primarily focused on increasing the supply of the precursor acetyl-CoA, upregulating the FFA biosynthetic pathway, and blocking competitive or degradative pathways[21,48]. Considering that microbial biosynthesis is embedded within interwoven cellular networks, many potential determinants could unexpectedly enhance product synthesis through distant genetic effects or unknown regulatory interactions. In a

https://doi.org/10.1038/s41467-025-58368-3

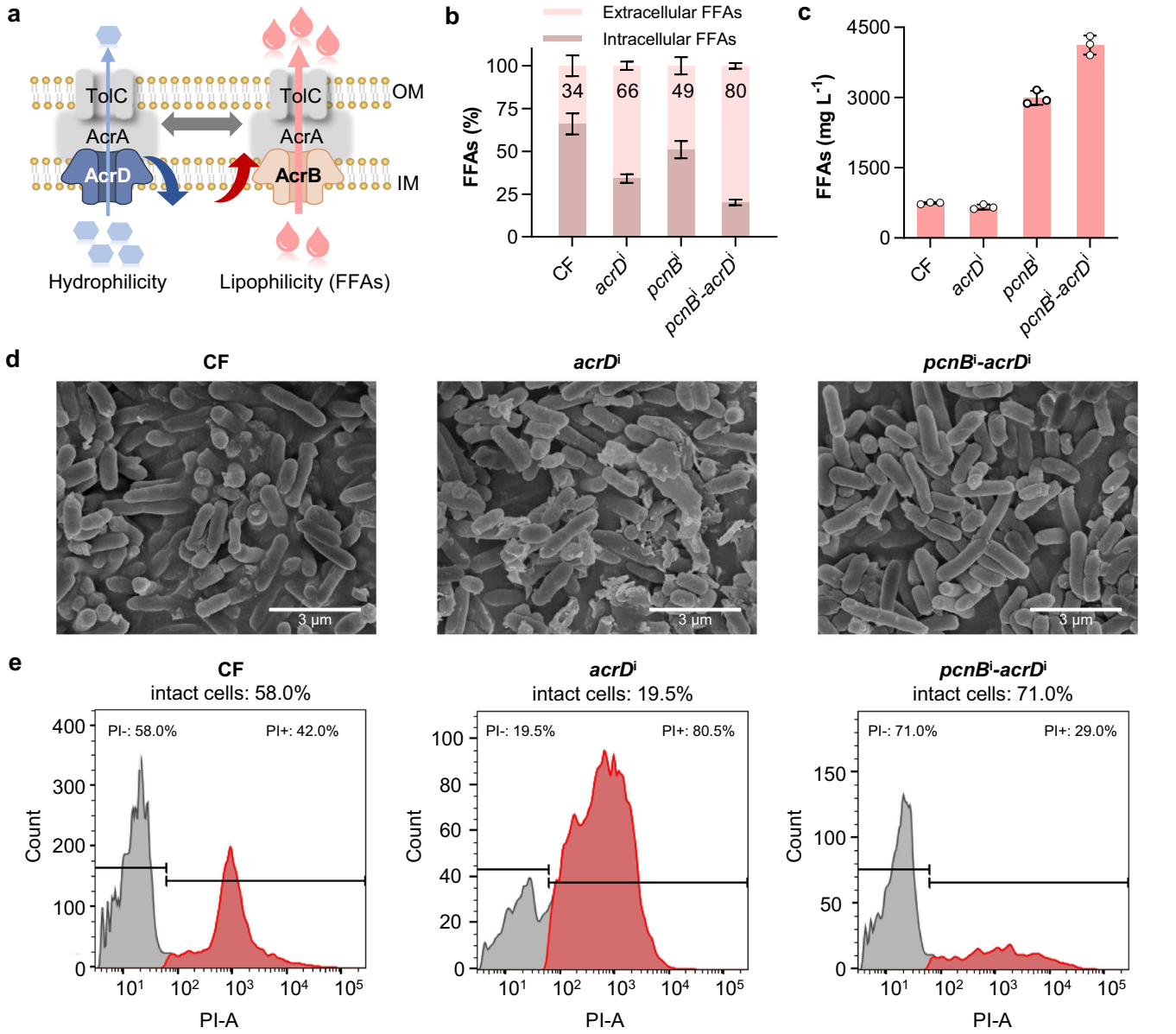

Fig. 6 | *acrD* repression increases FFAs production by enhancing efflux based on synergistic repression of *pcnB*. **a** Schematic illustration depicting that reducing the AcrD level potentially frees up more available TolC and AcrA for interaction with AcrB, thereby enhancing the efflux of lipophilic FFAs. OM, Outer membrane. IM, Inner membrane. **b** *acrD* repression increases the percentage of extracellular FFAs. **c** FFAs production is increased by *acrD* repression on the basis of *pcnB* repression but is decreased by *acrD* repression alone compared to the CF strain. **d** Cell surface damage caused by *acrD* repression is alleviated by *pcnB* repression. Samples were collected after 12 h of IPTG induction and cell surface was detected using SEM. **e** Membrane integrity damage resulting from *acrD* repression is also alleviated by *pcnB* repression. Samples were collected after 12 h of IPTG induction. Membrane integrity was represented by the percentage of intact cells, which was detected by propidium iodide (PI) staining and flow cytometry. These experiments in (**d**, **e**) were repeated three times with similar results. Data are presented as mean ± SD ($n = 3$ biological replicates). Source data are provided as a Source Data file.

previous study, we combined the CRISPRi system with omics analysis to identify beneficial genes for FFAs production[19]. We used CRISPRi to repress genes in competitive pathways or transcriptional factors to improve FFAs production. The strain targeting each gene was constructed one by one and fermented individually, and a limited set of only 108 genes was modulated. To identify potential targets hidden within the cellular network, we conducted transcriptomic and proteomic analyses of three engineered strains and targeted 41 co-differentially expressed genes for FFAs production. Ultimately, the FFAs titer was increased to 2901 mg L^{-1} through combinatorial modulation of four identified genes, two from CRISPRi perturbation and two from omics analyses. Overall, the entire process was relatively time-consuming and labor-intensive, and this approach merely touched upon a small fraction of the genome. By comparison, this study extends the scope of targeted genes to the entire genome through a pooled CRISPRi library combining high-throughput FACS and NGS analysis. As such, we identified a beneficial gene target, *pcnB*, in the first round of screening, whose single repression resulted in FFAs titer of 2992 mg L^{-1} (Fig. 1), surpassing that of the best-engineered strain combinatorial perturbation of four genes in our previous study[19]. Due to its effectiveness and flexibility, CRISPR-based genome-scale screening has been applied to other contexts, such as DNA damage response and membrane trafficking[49,50]. Notably, this study represents a significant application of genome-scale CRISPRi screening for FFAs overproduction and allows for exploring the complex cellular network for enhanced FFAs production.

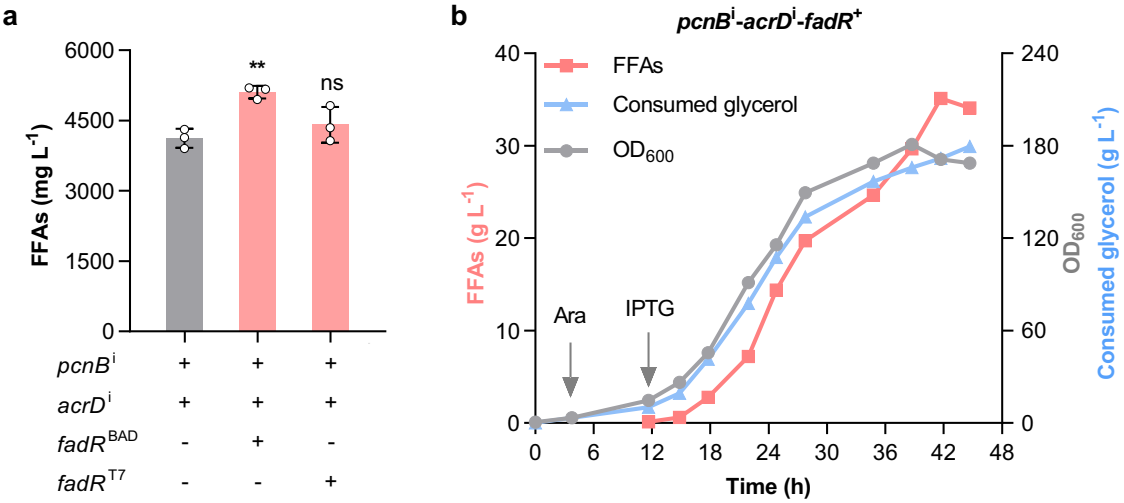

Fig. 7 | Fermentation of the *pcnB*^{i}-*acrD*^{i}-*fadR*$^{+}$ strain. a FFAs production is enhanced by further overexpressing *fadR* using the P_{BAD} promoter in the *pcnB*^{i}-*acrD*^{i} strain (the recombinant strain named *pcnB*^{i}-*acrD*^{i}-*fadR*$^{+}$) in tube fermentation. Data are presented as mean ± SD ($n = 3$ biological replicates). The *P*-value is calculated with an unpaired two-tailed *t*-test, where ns represents not significant; $^{**}P = 0.0022$ and $P = 0.3071$ (ns) comparing the *fadR*-overexpressing strain vs. *pcnB*^{i}-*acrD*^{i}. **b** Fed-batch fermentation of the *pcnB*^{i}-*acrD*^{i}-*fadR*$^{+}$ strain in a 5 L bioreactor achieves the highest FFAs titer of 35.1 g L^{-1} at 41.7 h. Arabinose was added at 3.8 h to induce *fadR* overexpression, and IPTG was added at 11.7 h to induce the overexpression of *tesA'* and the repression of *pcnB* and *acrD*. Ara, Arabinose. IPTG, Isopropyl β-D-thiogalactopyranoside. Source data are provided as a Source Data file.

In this study, we achieved, as far as we are aware, the maximum FFAs titer in *E. coli* (35.1 g L^{-1}) and the highest productivity of FFAs production through microbial fermentation (0.84 g L^{-1} h^{-1}) reported to date. This FFAs titer surpasses those of oleaginous *Yarrowia lipolytica* (9.67 g L^{-1})[51] and *Pichia pastoris* (23.4 g L^{-1})[52], is comparable to *Saccharomyces cerevisiae* (33.4 g L^{-1})[53] and *Ogataea polymorpha* (38.2 g L^{-1})[54], although it is below that of oleaginous *Rhodococcus opacus* (50.2 g L^{-1})[55] (Supplementary Table 1). Notably, the FFAs productivity of our engineered *E. coli* strain is over 5-fold that of the engineered yeasts[51–54] and even 1.76-fold that of the engineered *Rhodococcus opacus*[55] (Supplementary Table 1). These results highlight the considerable potential of *E. coli* as a robust host for FFAs production and demonstrate the substantial effectiveness of our genome-scale screening efforts in enhancing microbial biosynthesis.

In summary, our results demonstrated that *pcnB* repression confers improved physiology for FFAs overproduction in *E. coli*. Although microbial physiology is highly complex, our genome-scale screen underscores the significance of identifying beneficial genetic determinants for engineering physiology. We can envision that physiology-oriented engineering would be expected to have promoting effects on the biosynthesis of other products as well.

Methods

Strains, plasmids, and medium

All strains and plasmids used in this study are listed in Supplementary Data 1 and Supplementary Data 2, respectively. The *fadE* and *pcnB* genes of *E. coli* MG1655(DE3) were deleted using the λ-RED recombineering system[56]. E108A and N138H were constructed using the CRISPR method referring to the previous study[25]. Plasmid construction was performed using the Golden Gate assembly method[57], restriction digestion and ligation, or the Basic Seamless Cloning and Assembly Kit (CU201, TransGen Biotech, China). Primers annealed to custom-designed spacers are listed in Supplementary Data 3. LB medium (5 g L^{-1} yeast extract, 10 g L^{-1} tryptone, and 10 g L^{-1} NaCl) was used for regular cultures of *E. coli* strains. Modified M9 medium[58] (pH 7.2) for tube and flask fermentation was prepared as follows: 17.1 g L^{-1} $Na_2HPO_4{\cdot}12H_2O$, 3 g L^{-1} KH_2PO_4, 0.5 g L^{-1} NaCl, 2 g L^{-1} NH_4Cl, 2 g L^{-1} yeast extract, 30 g L^{-1} glycerol (or 30 g L^{-1} glucose, specifically used in Fig. 4), 0.25 g L^{-1} $MgSO_4{\cdot}7H_2O$, 11.1 mg L^{-1} $CaCl_2$, 10 mg L^{-1} thiamine, 0.1% (v/v) Triton-X100, and 1 mL L^{-1} metal trace stock solution. The metal trace stock solution contained 27 g L^{-1} $FeCl_3{\cdot}6H_2O$, 2 g L^{-1} $ZnCl_2$, 2 g L^{-1} $Na_2MoO_4{\cdot}2H_2O$, 1.9 g L^{-1} $CuSO_4{\cdot}5H_2O$, and 0.5 g L^{-1} H_3BO_3. Modified mineral medium[58] (pH 7.2) for fed-batch fermentation contained 6 g L^{-1} NH_4Cl, 8.5 g L^{-1} KH_2PO_4, 0.5 g L^{-1} citrate, 5 g L^{-1} yeast extract, 15 g L^{-1} glycerol, 1 g L^{-1} $MgSO_4{\cdot}7H_2O$, 0.07 g L^{-1} $CaCl_2{\cdot}2H_2O$, 4 mL L^{-1} metal trace stock solution, and 100 mg L^{-1} thiamine. The feeding medium for fed-batch fermentation contained 2.47 g L^{-1} $MgSO_4{\cdot}7H_2O$, 500 g L^{-1} glycerol, and 100 g L^{-1} yeast extract. If necessary, 34 μg mL^{-1} chloramphenicol or 100 μg mL^{-1} ampicillin was supplemented.

Cultivation and fermentation

Glass-tube fermentations were carried out in 5 mL of modified M9 medium. Each strain was inoculated from a freshly transformed single colony on an LB agar plate into 2 mL of LB medium (with the corresponding antibiotic). When cell density reached the stationary phase, 1% (v/v) of culture was re-inoculated into 5 mL of modified M9 medium (with the corresponding antibiotic) in a glass tube and cultivated at 250 rpm and 30 °C. The cultures were induced with 1 mM IPTG at an OD_{600} of approximately 1 and allowed to grow for an additional 40 h. When the P_{BAD} promoter was used, 10 mM arabinose was utilized to induce gene expression at an OD_{600} of 0.5–0.6. Tube cultivations were performed in three biological replicates.

Shake-flask fermentations were implemented in 250 mL shake flasks containing 50 mL of modified M9 medium (with the corresponding antibiotic). Flask cultivations followed the same procedures as glass-tube fermentations and were performed in three biological replicates. For the CRISPRi screen, fermentations were performed in 500 mL shake flasks containing 100 mL of modified M9 medium. For more detailed information, please see the "Genome-scale CRISPRi screen" section.

Fed-batch fermentation for FFAs production was carried out in 2 L of modified mineral medium. The overnight LB culture (1 mL) of the freshly transformed single colony was re-inoculated into 100 mL of modified mineral medium (with chloramphenicol and ampicillin) in 500 mL shake flasks. When OD_{600} reached 3–4, 200 mL of culture was re-inoculated into a 5 L bioreactor (T&J, China) with 1.8 L of modified

mineral medium (with chloramphenicol and ampicillin). Fermentation temperature was set at 30 °C and pH was controlled at 7 by feeding 6 N ammonium hydroxide via an auto pump. The air flow rate was maintained at around 2 L min^{-1}. The dissolved oxygen (dO_2) concentration was controlled above 30% by agitation cascade (300–800 rpm). When cell density (OD_{600}) reached approximately 4 and 15, 10 mM arabinose and 1 mM IPTG was added to the fermentation culture, respectively. The feeding medium was added to the fermentation culture when the initial glycerol was almost depleted, as indicated by a sharp increase in the dO_2 concentration. The carbon source restriction strategy was controlled by monitoring the dO_2 concentration, with feeding automatically starting at 5 mL min^{-1} when dO_2 exceeded 50% and stopping when dO_2 fell below 50%. Antifoam has been added automatically as needed. Broth samples (about 5 mL) were collected at various time points to measure cell density and stored at −20 °C for subsequent measurements of glycerol and FFAs.

Genome-scale CRISPRi screen

For a schematic illustration of the genome-scale CRISPRi screen, refer to Fig. 1a. The CF strain carrying the pCF plasmid was cultured in 100 mL of LB medium containing the corresponding antibiotic to an OD_{600} of 0.6. Cultures were then prepared for electroporation by chilling on ice, washing four times with 10% glycerol, and resuspending in 4 mL of the same solution. The competent cells were mixed with the plasmid library (800 ng plasmid per mL of competent cells) and transferred to pre-chilled 0.2-cm electroporation cuvettes in 200 μL aliquots. Electroporation was performed using a MicroPulser System (Bio-Rad, USA) set to 2.1 kV, 0.6 kΩ, and 10 μF. Post-electroporation, cells were allowed to recover in LB broth (1:4, v/v) at 30 °C for 1.5 h, then collected and resuspended in 20 mL of fresh LB broth containing the corresponding antibiotic. Transformation efficiency was evaluated by diluting 50 μL of the culture, spreading it on LB agar plates containing the corresponding antibiotic, and counting colonies after overnight incubation at 30 °C. The results confirmed that the coverage was at least 20-fold. The remaining culture was grown to an OD_{600} of about 1. For NGS preparation, 5 mL of cell cultures (Tra1) were collected. The remaining part was re-inoculated into two 500 mL flasks containing 100 mL of modified M9 medium containing the corresponding antibiotic and cultivated with shaking at 30 °C and 250 rpm. Upon reaching an OD_{600} of about 1, cultures were induced with 1 mM IPTG and allowed to grow for an additional 40 h. Prior to sorting, 5 mL of cell cultures designated as before sorting (BS) was collected for NGS. In the second round of screening, the *pcnB*^{i} strain carrying the pCF-*pcnB*^{i} plasmid was utilized for competent cell preparation and electroporation of the plasmid library.

For cell sorting, 500 μL of culture was collected, washed twice with filtered PBS, and diluted to an OD_{600} of 0.2. The sample was then mixed with 20 μg mL^{-1} Nile Red (N121291, Aladdin, China) and incubated in the dark for 5 min for staining. The stained cells were further diluted to an OD_{600} of 0.1 and subjected to sorting using a FACSAria III cell sorter (BD, USA) equipped with a 488 nm laser for excitation and a 585 ± 42 nm filter for detection and FACSDiva software (v8.0.2). Forward scatter and side scatter were in logarithmic amplification, and a gate set on forward scatter versus side scatter was applied for cell collection. The top 1% of cells displaying the highest fluorescence intensity were sorted into the LB medium, collecting over eight thousand cells. Following recovery and cultivation, cell cultures designated as after sorting (AS) were collected for NGS.

NGS library preparation and sequencing

The plasmids in the transformed cell library (Tra1), cell library before sorting (BS), and cell library after sorting (AS) were extracted and used as templates to amplify the N20 region of library sgRNAs. The PCR conditions were set as follows: 50 μL × 2 reactions per library, 100 ng template per reaction, PF/R_pTargetLacNGS_PE150 (Supplementary Data 3), 2× Phanta Max Master Mix (P515, Vazyme, China), 95 °C 3 min, 25 cycles (95 °C, 15 s; 62 °C, 15 s; 72 °C, 30 s), 72 °C for 5 min. The purified PCR products were used for NGS library preparation and sequencing on an Illumina NovaSeq 6000 instrument using a 2 × 150 paired-end configuration, performed by GENEWIZ from Azenta Life Sciences Co., Ltd (China). In the first round of screening, the NGS data of samples from the transformed cell library, the cultivated cell library before sorting (BS), and the cell library after sorting (AS) were named Tra1, Cul2, and Sor3, respectively. In the second round of screening, the NGS data of samples from BS and AS were named B-cul2 and B-sor3-P5, respectively.

The raw NGS data were processed by GENEWIZ from Azenta Life Sciences Co., Ltd (China). The N20 sequences were extracted using standard bioinformatics methods and then mapped back to the sgRNA library, through which the read count for each sgRNA in each library was determined. The NGS data generated in this study have been deposited in the NCBI GEO database under accession code GSE267827. Reads per sgRNA ($reads_{sgRNA}+1$) were normalized to the total number of reads per sample (total $reads_{total}$) to calculate the relative abundance of sgRNAs (normalized $reads_{sgRNA}$) (Eq. 1). Fitness of each sgRNA was calculated by dividing the normalized reads for this sgRNA in the cell library after sorting (AS) by the normalized reads in the cell library before sorting (BS) and subsequently taking the $\log_2$ value (Eq. 2). In fitness calculation for each sgRNA, the relative abundance before sorting (normalized reads in BS) was processed as 1. Thus, fitness reflects the relative abundance of each sgRNA due solely to sorting, helping to minimize data noise from cultivation. sgRNAs with fewer than 20 reads in each library were excluded from the analysis to calculate sgRNA fitness.

$$\text{Normalized reads}_{sgRNA} = \frac{\text{Reads}_{sgRNA}+1}{\text{Total reads}} \tag{1}$$

$$\text{Fitness}_{sgRNA} = \log_2\left(\frac{\text{Normalized reads}_{sgRNA}\text{ in AS}}{\text{Normalized reads}_{sgRNA}\textit{ in BS}}\right) \tag{2}$$

Metabolite extraction and analysis

FFAs were extracted and quantified following previously published methods[59]. Specifically, 0.5 mL of cell culture (or an appropriate volume of cell culture diluted to 0.5 mL) was acidified with 50 μL of concentrated HCl, spiked with 100 μg of heptadecanoic acid (H114399, Aladdin, China) as internal standard. The cell culture was extracted twice with 0.5 mL of ethyl acetate (E116136, Aladdin, China). For intracellular FFAs extraction, 0.5 mL cell culture was centrifuged at 10,000 × *g* for 5 min to separate the supernatant and the cell pellet. The cell pellet was resuspended with 0.5 mL distilled water and then extracted following the same procedure described above. The extracted FFAs were then determined using a Thermo Scientific TRACE 1300 gas chromatograph (GC) equipped with a TG-WaxMS A column (30 m × 0.32 mm × 0.25 μm; Thermo Fisher Scientific, USA) and a Flame Ionization Detector (FID) operating under a constant flow rate of the carrier gas (nitrogen) at 1 mL min^{-1}. The following temperature program was used: hold at 50 °C for 1 min, then heat to 245 °C at 30 °C min^{-1} and hold at this temperature for 22.5 min. Individual fatty acid species were qualified by authentic homologous standards and quantified by comparing the peak areas with that of the internal standard using the Chromeleon software (v7.1). Total concentrations of FFAs were calculated as the sum of C_{12} to C_{18} (saturated and monounsaturated).

Glycerol and fermentation byproducts were determined by high-performance liquid chromatography (HPLC) following Waters standard protocols. Briefly, filtered culture supernatants were analyzed by a Waters HPLC system including a Waters e2695 separation module

and an Aminex HPX-87H column (300 mm × 7.8 mm, Catalog no. 1250140, Bio-Rad, USA). The separation was performed through elution with 5 mM H_2SO_4 at a flow rate of 0.5 mL min^{-1} at 60 °C for 30 min. Pyruvate, succinate, lactate, formate, and acetate were detected by a Waters 2998 photodiode array detector (PDA) with a wavelength of 210 nm. Glycerol was detected by a Waters 2414 refractive index detector (RID). Concentration calculation was conducted by comparing the peak areas with the standard using the Empower software (v3).

Transcriptomic analysis

Cells from the CF (control) and *pcnB*^{i} strains (three biological replicates for each) were harvested during the exponential phase with high gene transcription activity (12 h after IPTG induction) by quick centrifugation at 4 °C and 10,000 × *g* for 1 min and immediately frozen in liquid nitrogen. The transcriptomic analysis was performed by BGI Genomics Co., Ltd (China). Briefly, total RNA was extracted using the RiboPure™ Bacteria Kit (AM1925, Invitrogen, USA) following the manufacturer's recommendations. RNA quality was checked using the DNF-471 Standard Sensitivity RNA Analysis Kit (DNF-471-0500, Agilent, USA) and running on Fragment Analyzer (Agilent, USA). RNA sample was treated with DNase-I to remove DNA and was subjected to TIANSeq rRNA Depletion Kit (G^- Bacteria) (NR101-T5A, TIANGEN, China) to remove rRNA. Sequencing libraries were constructed using the Optimal Dual-mode mRNA Library Prep Kit (LR00R96, BGI, China) following the manufacturer's instructions. Circularization was performed using the MGIEasy Circularization Kit (1000005259, MGI, China) and the product was quantitated using the Qubit® ssDNA Assay Kit (Q10212, Invitrogen, USA). The libraries were then prepared using the MGISEQ-2000RS High-throughput Sequencing Set (FCL PE100) (1000012554, MGI, China) and sequenced via the DNBSEQ-G400 platform (BGI, China) according to the manufacturer's instructions. Differential expression analysis was performed using DESeq2[60] (v1.4.5) with *q*-value < 0.05 as the threshold for significance. KEGG enrichment analysis was performed using Phyper based on the Hypergeometric test with *Q*-value < 0.05 as the threshold for significance. The transcriptomics data generated in this study have been deposited in the NCBI GEO database under accession code GSE267710. A and AP represent the CF and *pcnB*^{i} strains, respectively.

Proteomic analysis

Cells from the CF (control) and *pcnB*^{i} strains (three biological replicates for each) were harvested by centrifugation at 4 °C and 5000 × *g* for 5 min at 24 h after IPTG induction and immediately frozen in liquid nitrogen. The sampling time for proteomic analysis was later than that for transcriptomic analysis, allowing time for changes in transcript levels to be translated and reflected in the functional proteins. The proteomic analysis was performed by BGI Genomics Co., Ltd (China). For protein preparation, cells were resuspended in lysis buffer with SDS L3 and Cocktail (including EDTA), then added with 10 mM dithiothreitol (DTT) and ground with a grinder and steel balls. After centrifugation, the supernatant was subjected to protein precipitation by vortexing with pre-cooled acetone. After centrifugation, the total precipitate was collected, dried, re-dissolved in lysis buffer without SDS L3, treated with ice bath ultrasound, and then centrifugated to get the supernatant. The sample was reduced with 10 mM DTT for 1 h at 56 °C and then alkylated with sufficient iodoacetamide for 1 h at room temperature in the dark. Samples were subjected to protein precipitation by vortexing with pre-cooled acetone. After centrifugation, the total precipitate was collected, dried, re-dissolved in lysis buffer without SDS L3, ground with a grinder, and then centrifugated to get the supernatant, which is the protein solution. The protein samples were quantitated by the Bradford method and detected by SDS-PAGE. 100 μg of each sample was digested with trypsin (90058, Thermo Fisher Scientific, USA) for 4 h, and the enzymatic peptides were desalted and vacuumed to dryness.

Equal amounts of peptides of each sample were mixed and diluted with mobile phase A (5% acetonitrile (ACN)). The sample was subjected to a high pH C18 column (4.6 × 250 mm, 5 μm) (Gemini, USA) using the LC-20AD HPLC system (Shimadzu, Japan) and eluted at a flow rate of 1 mL min^{-1} by the following gradient: 5% mobile phase B (95% ACN) for 10 min, 5%–35% mobile phase B for 40 min, 35%–95% mobile phase B for 1 min, mobile phase B for 3 min, and 5% mobile phase B for 10 min. The elution peak was monitored at a wavelength of 214 nm and the component was collected every minute. Components were combined into 10 fractions and then freeze-dried. The dried peptide samples were reconstituted with mobile phase A (2% ACN, 0.1% formic acid (FA)) and centrifuged at 20,000 × *g* for 10 min. The supernatant was taken for separation by an UltiMate 3000 UHPLC (Thermo Fisher Scientific, USA) with a tandem self-packed C18 column (150 μm × 35 cm, 1.8 μm) and eluted at a flow rate of 500 nL min^{-1} by the following gradient: 5% mobile phase B (98% ACN, 0.1% FA) for 5 min, 5%–25% mobile phase B for 115 min, 25%–35% mobile phase B for 40 min, 35%–80% mobile phase B for 10 min, 80% mobile phase B for 5 min, and 5% mobile phase B for 5 min. The separated peptides were ionized by a nanoESI source and then passed to a tandem mass spectrometer (MS) Orbitrap Exploris 480 (Thermo Fisher Scientific, USA) for Data Dependent Acquisition (DDA) mode detection. The main parameters were set as follows: 1.9 kV ion source voltage, MS 350-1650 m/z scanning range, 120,000 resolution, 300% automatic gain control (AGC), 90 ms maximal injection time (MIT); MS/MS collision type HCD, collision energy NCE 30, 30,000 resolution, 100% AGC, 120 s dynamic exclusion duration, and MIT was auto mode. Precursor for MS/MS scan satisfied: charge range 2+ to 6+, top 30 precursors with intensity over 2E4.

The dried peptides for each sample were reconstituted with mobile phase A (2% ACN, 0.1% FA) and centrifuged at 20,000 × *g* for 10 min. The supernatant was taken for separation by an UltiMate 3000 UHPLC (Thermo Fisher Scientific, USA) with a tandem self-packed C18 column (150 μm × 35 cm, 1.8 μm) and eluted at a flow rate of 500 nL min^{-1} by the following gradient: 5% mobile phase B (98% ACN, 0.1% FA) for 5 min, 5% –25% mobile phase B for 85 min, 25%–35% mobile phase B for 10 min, 35%–80% mobile phase B for 8 min, 80% mobile phase B for 5 min, and 5% mobile phase B for 7 min. The separated peptides were ionized by a nanoESI source and then passed to a tandem MS Orbitrap Exploris 480 (Thermo Fisher Scientific, USA) for Data Independent Acquisition (DIA) mode detection. The main parameters were set as follows: 1.9 kV ion source voltage, MS 400-1250 m/z scanning range, 120,000 resolution, 300% AGC, 90 ms MIT, 400-1250 m/z was equally divided to 50 continuous windows MS/MS scan. MS/MS collision type HCD, collision energy NCE 30, 30,000 resolution, 1000% AGC, and MIT was auto mode.

DDA data were identified using MaxQuant[61] (v1.5.3.30) against the *Escherichia coli* str. K-12 substr. MG1655 RefSeq protein database (updated on 26-09-2013) in the National Center for Biotechnology Information (NCBI). Peptide/protein entries that satisfied False Discovery Rate (FDR) < 1% were used to build the final spectral library. Parameters were selected as follows: trypsin digestion, maximum of two missed cleavages allowed, minimal peptide length of 7, peptide-spectrum match (PSM) and protein FDR < 0.01, fixed modifications are carbamidomethyl, variable modifications are methionine oxidation and N-terminal acetylation. DIA data was analyzed using Spectronaut[62] (v17.0), which uses iRT peptides to calibrate retention time. FDR was estimated using the mProphet scoring algorithm, which accurately reflects the matching degree of ion pairs. Differential protein expression analysis was performed using MSstats[63] with *p*-value < 0.05 as the threshold for significance. KEGG enrichment analysis was based on the Hypergeometric test with a *P*-value < 0.05 as the threshold for significance. The mass spectrometry proteomics data generated in this study have been deposited in the ProteomeXchange Consortium under accession code

PXD052390. A and AP represent the CF and *pcnB*^{i} strains, respectively.

RT-qPCR and RNA stability analysis

Samples were collected at 3 h after IPTG induction to assess the relatively immediate responses of gene expression upon CRISPRi-mediated transcriptional repression. Other time points after 3 h of induction (Fig. 1f) were sampled for RT-qPCR assay to track the effectiveness of CRISPRi. Total RNA was extracted using the U-Fast Bacterial RNA Extraction Kit (ZP431, Zoman, China). The total RNA of each sample (1 μg) was reversely transcribed to complementary DNA (cDNA) using the RevertAid First Strand cDNA Synthesis Kit (K1622, Thermo Fisher Scientific, USA) and random hexamer primer according to the manufacturer's protocol. RT-qPCR was performed with gene-specific primers following the instructions of 2× Universal SYBR Green Fast qPCR Mix (RK21203, ABclonal, China) in a Quantagene q225 system (Kubotech, China) with q225 software (v3.19.3.1501). The expression level for each gene in the engineered strain was calculated by normalizing to the 16S rRNA gene and relative to that of the CF strain using the ΔΔCT method[64].

For RNA stability measurement, cells at 12 h after IPTG induction were treated with 500 μg/mL rifampicin to inhibit transcription. Time 0 (t = 0 min) was set 1 min after adding rifampicin. Samples were collected at multiple time points (t = 0, 1, 2, 4, 6, 8, 12, 16, 24 min). The total RNA of each sample was extracted and applied to RT-qPCR. The stability of specific RNA was measured by following the decrease in % RNA level over time with 0 time point taken as 100% of each gene expression[34]. Primers used for RT-qPCR analysis are listed in Supplementary Data 3.

3′-RACE assay

Samples were collected at 3 h after IPTG induction, and total RNA was extracted using the U-Fast Bacterial RNA Extraction kit (ZP431, Zoman, China). The total RNA of each sample was reversely transcribed to cDNA using the oligo(dT)-containing adapter primer (AP). cDNA was further utilized as the template for PCR amplification using gene-specific forward primer and abridged universal amplification primer (AUAP). If DNA fragments can be amplified using the *gadX*, *gadE*, *osmY*, or *dxs* forward primers, the size will be slightly larger than 433, 313, 394, and 477 bp, respectively. PCR products were separated by 1% agarose gel electrophoresis to observe the specific DNA band. Primers used for the 3′-RACE assay are listed in Supplementary Data 3.

Membrane determination

Membrane integrity was assessed using propidium iodide (PI, P422887, Aladdin, China) staining and flow cytometry detection. Cells were collected at 12 h after IPTG induction (during the exponential phase with high activity in physiological responses) by centrifugation at 5000 × g for 2 min. The cell pellet was washed twice with cold PBS and resuspended to an OD_{600} of 0.4. Cells were then stained with PI to a final concentration of 2 μg mL^{-1} for 10 min at room temperature in the dark. PI fluorescence was measured using a FACSAria III cell sorter (BD, USA) (488/616 nm) and FACSDiva software (v8.0.2). Cells without PI staining were adopted to define the negative boundary. In the subsequent experiments, the same boundary and gating strategy was copied to calculate PI-positive (PI+) and PI-negative (PI-) cells. Data analysis was performed using FlowJo software (v10.8.1).

Cell surface hydrophobicity was assessed following the MATH method[65]. Cells were harvested at 12 h after IPTG induction by centrifugation at 5000 × g for 2 min. The cell pellet was washed twice and resuspended in PBS buffer at a final OD_{600} of about 0.6. The OD_{600} value of cell suspension (OD1) was measured using a Synergy H1 microplate reader (Biotek, USA) and Gen5 CHS software (v3.08). Then, 1 mL of dodecane (D108176, Aladdin, China) was added to 4 mL of the cell suspension, and the mixture was vortexed for 10 min. The mixtures were left to settle for 15 min, and the OD_{600} value of the aqueous phase (OD2) was measured. Cell surface hydrophobicity was calculated using the following equation: percent partitioning = (OD1-OD2)/OD1 × 100.

Intracellular ROS and ATP Assay

Intracellular ROS was assessed by the Reactive Oxygen Species Assay Kit (S0033S, Beyotime, China), following the manufacturer's instructions. Cells were collected at 12 h after IPTG induction and washed twice with PBS buffer. 0.1 OD_{600} cells were then resuspended in 500 μL PBS buffer containing 10 μM 2,7-Dichlorofluorescein diacetate (DCFDA), incubated at 37 °C in the dark for 20 min, and then washed trice with PBS buffer. Finally, the fluorescence of each sample was detected using a Synergy H1 microplate reader (Biotek, USA) with an excitation wavelength of 488 nm and an emission wavelength of 525 nm and Gen5 CHS software (v3.08). The fluorescence of each sample was also imaged using a fluorescence microscope BX53 (Olympus, Japan) and ImageAnalysisSystem software (v11).

Intracellular ATP was measured by the Enhanced ATP Assay Kit (S0027, Beyotime, China), following the manufacturer's instructions. Cells were collected at 12 h and 24 h after IPTG induction by centrifugation at 4 °C and 5000 × g for 2 min. To maintain the stability of ATP, the entire process was carried out in an ice bath. The pellets were resuspended in 200 μL lysate solution, lysed by an ultrasonic cell-crushing device on an ice-cold holder, and then centrifuged at 4 °C and 10,000 × g for 5 min. The supernatant was mixed with the working solution, and the chemiluminescence value was measured using a Synergy H1 microplate reader (Biotek, USA) and Gen5 CHS software (v3.08).

SEM analysis

SEM analysis was performed to observe modifications on the cell surface of the CF, *acrD*^{i}, and *pcnB*^{i}-*acrD*^{i} strains. Cells were collected at 12 h after IPTG induction by centrifugation at 5000 × g for 5 min. The pellets were washed thrice with PBS buffer and fixed in 2.5% (v/v) glutaraldehyde solution (G105907, Aladdin, China) at 4 °C for 6 h. The cells were washed thrice with PBS buffer and then fixed with 1% osmium tetraoxide (O111788, Aladdin, China) for 2 h. The fixed cells were washed thrice with PBS buffer and then dehydrated at varying concentrations with ethanol (20%, 40%, 60%, 80%, 100%). Finally, critically dried samples were analyzed by the Regulus8100 SEM (Hitachi, Japan).

Statistics and reproducibility

Quantitative data of three biological replicates are presented as mean ± SD, as indicated in legends of figures. Statistical analysis was conducted using the unpaired two-tailed Student's t-test. Significance levels are indicated as $^{*}P < 0.05$, $^{**}P < 0.01$, $^{***}P < 0.001$, $^{****}P < 0.0001$; ns, non-significant. Statistical calculations were performed using GraphPad Prism (v8.3.0). No statistical method was used to predetermine sample size, and no data was excluded from the analysis.

Reporting summary

Further information on research design is available in the Nature Portfolio Reporting Summary linked to this article.

Data availability

The NGS data and transcriptomics data generated in this study have been deposited in the NCBI GEO database under accession codes GSE267827 and GSE267710, respectively. The mass spectrometry proteomics data generated in this study have been deposited in the ProteomeXchange Consortium under accession code PXD052390. Other data supporting the findings of this study are available within the

article, Supplementary Information files, and Source Data files linked to each figure. Source data are provided with this paper.

References

1. Choi, K. R. et al. Systems metabolic engineering strategies: integrating systems and synthetic siology with metabolic engineering. *Trends Biotechnol.* **37**, 817–837 (2019).
2. Nielsen, J. & Keasling, J. D. Engineering cellular metabolism. *Cell* **164**, 1185–1197 (2016).
3. Ko, Y. S. et al. Tools and strategies of systems metabolic engineering for the development of microbial cell factories for chemical production. *Chem. Soc. Rev.* **49**, 4615–4636 (2020).
4. Zhang, Y., Zhu, Y., Zhu, Y. & Li, Y. The importance of engineering physiological functionality into microbes. *Trends Biotechnol.* **27**, 664–672 (2009).
5. Liu, H. et al. Microbial physiological engineering increases the efficiency of microbial cell factories. *Crit. Rev. Biotechnol.* **41**, 339–354 (2021).
6. Montano Lopez, J., Duran, L. & Avalos, J. L. Physiological limitations and opportunities in microbial metabolic engineering. *Nat. Rev. Microbiol.* **20**, 35–48 (2022).
7. Robertson, J. L. The lipid bilayer membrane and its protein constituents. *J. Gen. Physiol.* **150**, 1472–1483 (2018).
8. Qi, Y., Liu, H., Chen, X. & Liu, L. Engineering microbial membranes to increase stress tolerance of industrial strains. *Metab. Eng.* **53**, 24–34 (2019).
9. Guo, L. et al. Engineering *Escherichia coli* lifespan for enhancing chemical production. *Nat. Catal.* **3**, 307–318 (2020).
10. Huo, K., Zhao, F., Zhang, F., Liu, R. & Yang, C. Morphology engineering: a new strategy to construct microbial cell factories. *World J. Microbiol. Biotechnol.* **36**, 127 (2020).
11. Imlay, J. A. The molecular mechanisms and physiological consequences of oxidative stress: lessons from a model bacterium. *Nat. Rev. Microbiol.* **11**, 443–454 (2013).
12. Shimizu, K. & Matsuoka, Y. Redox rebalance against genetic perturbations and modulation of central carbon metabolism by the oxidative stress regulation. *Biotechnol. Adv.* **37**, 107441 (2019).
13. Lennen, R. M. & Pfleger, B. F. Microbial production of fatty acid-derived fuels and chemicals. *Curr. Opin. Biotechnol.* **24**, 1044–1053 (2013).
14. Marella, E. R., Holkenbrink, C., Siewers, V. & Borodina, I. Engineering microbial fatty acid metabolism for biofuels and biochemicals. *Curr. Opin. Biotechnol.* **50**, 39–46 (2018).
15. Tan, Z., Black, W., Yoon, J. M., Shanks, J. V. & Jarboe, L. R. Improving *Escherichia coli* membrane integrity and fatty acid production by expression tuning of FadL and OmpF. *Micro. Cell Fact.* **16**, 38 (2017).
16. Liu, H. et al. Enhancing biofuels production by engineering the actin cytoskeleton in *Saccharomyces cerevisiae*. *Nat. Commun.* **13**, 1886 (2022).
17. Shin, K. S. & Lee, S. K. Increasing extracellular free fatty acid production in *Escherichia coli* by disrupting membrane transport systems. *J. Agric. Food Chem.* **65**, 11243–11250 (2017).
18. Royce, L. A. et al. Evolution for exogenous octanoic acid tolerance improves carboxylic acid production and membrane integrity. *Metab. Eng.* **29**, 180–188 (2015).
19. Fang, L. et al. Genome-scale target identification in *Escherichia coli* for high-titer production of free fatty acids. *Nat. Commun.* **12**, 4976 (2021).
20. Wang, T. et al. Pooled CRISPR interference screening enables genome-scale functional genomics study in bacteria with superior performance. *Nat. Commun.* **9**, 2475 (2018).
21. Xu, P. et al. Modular optimization of multi-gene pathways for fatty acids production in *E. coli*. *Nat. Commun.* **4**, 1409 (2013).
22. Xiao, Y., Bowen, C. H., Liu, D. & Zhang, F. Exploiting nongenetic cell-to-cell variation for enhanced biosynthesis. *Nat. Chem. Biol.* **12**, 339–344 (2016).
23. Yao, L. et al. Pooled CRISPRi screening of the cyanobacterium *Synechocystis* sp PCC 6803 for enhanced industrial phenotypes. *Nat. Commun.* **11**, 1666 (2020).
24. Cui, L. et al. A CRISPRi screen in *E. coli* reveals sequence-specific toxicity of dCas9. *Nat. Commun.* **9**, 1912 (2018).
25. Koleski, E. J. *Adaptive Cellular Strategies to Improve Commodity Chemical Production in Escherichia coli*. Doctor, Univ. California, Berkeley (2023).
26. Cao, G. J. & Sarkar, N. Identification of the gene for an *Escherichia coli* poly(A) polymerase. *Proc. Natl Acad. Sci. USA* **89**, 10380–10384 (1992).
27. Blum, E., Carpousis, A. J. & Higgins, C. F. Polyadenylation promotes degradation of 3′-structured RNA by the *Escherichia coli* mRNA degradosome in vitro. *J. Biol. Chem.* **274**, 4009–4016 (1999).
28. Mohanty, B. K. & Kushner, S. R. Analysis of the function of *Escherichia coli* poly(A) polymerase I in RNA metabolism. *Mol. Microbiol.* **34**, 1094–1108 (1999).
29. Mohanty, B. K. & Kushner, S. R. The majority of *Escherichia coli* mRNAs undergo post-transcriptional modification in exponentially growing cells. *Nucleic Acids Res.* **34**, 5695–5704 (2006).
30. Tramonti, A., Visca, P., De Canio, M., Falconi, M. & De Biase, D. Functional characterization and regulation of *gadX*, a gene encoding an AraC/XylS-like transcriptional activator of the *Escherichia coli* glutamic acid decarboxylase system. *J. Bacteriol.* **184**, 2603–2613 (2002).
31. Hommais, F. et al. GadE (YhiE): a novel activator involved in the response to acid environment in *Escherichia coli*. *Microbiology* **150**, 61–72 (2004).
32. Urban, J. H. & Vogel, J. Two seemingly homologous noncoding RNAs act hierarchically to activate *glmS* mRNA translation. *PLoS Biol.* **6**, e64 (2008).
33. Francis, N. & Laishram, R. S. Transgenesis of mammalian PABP reveals mRNA polyadenylation as a general stress response mechanism in bacteria. *iScience* **24**, 103119 (2021).
34. Sudheesh, A. P., Mohan, N., Francis, N., Laishram, R. S. & Anderson, R. A. Star-PAP controlled alternative polyadenylation coupled poly(A) tail length regulates protein expression in hypertrophic heart. *Nucleic Acids Res.* **47**, 10771–10787 (2019).
35. De Biase, D. & Pennacchietti, E. Glutamate decarboxylase-dependent acid resistance in orally acquired bacteria: function, distribution and biomedical implications of the *gadBC* operon. *Mol. Microbiol.* **86**, 770–786 (2012).
36. Jarboe, L. R., Royce, L. A. & Liu, P. Understanding biocatalyst inhibition by carboxylic acids. *Front. Microbiol.* **4**, 272 (2013).
37. Vind, J., Sorensen, M. A., Rasmussen, M. D. & Pedersen, S. Synthesis of proteins in *Escherichia coli* is limited by the concentration of free ribosomes: expression from reporter genes does not always reflect functional mRNA levels. *J. Mol. Biol.* **231**, 678–688 (1993).
38. Oyarzun, D. A., Chaves, M. & Hoff-Hoffmeyer-Zlotnik, M. Multistability and oscillations in genetic control of metabolism. *J. Theor. Biol.* **295**, 139–153 (2012).
39. Royce, L. A. et al. Transcriptomic analysis of carboxylic acid challenge *in Escherichia coli*: beyond membrane damage. *PLoS ONE* **9**, e89580 (2014).
40. Foster, J. W. *Escherichia coli* acid resistance: tales of an amateur acidophile. *Nat. Rev. Microbiol.* **2**, 898–907 (2004).
41. Guan, N. & Liu, L. Microbial response to acid stress: mechanisms and applications. *Appl. Microbiol. Biotechnol.* **104**, 51–65 (2020).
42. Mols, M., van Kranenburg, R., van Melis, C. C., Moezelaar, R. & Abee, T. Analysis of acid-stressed *Bacillus cereus* reveals a major oxidative response and inactivation-associated radical formation. *Environ. Microbiol.* **12**, 873–885 (2010).

43. Claus, S., Jezierska, S. & Van Bogaert, I. N. A. Protein-facilitated transport of hydrophobic molecules across the yeast plasma membrane. *FEBS Lett.* **593**, 1508–1527 (2019).
44. Garst, A. D. et al. Genome-wide mapping of mutations at single-nucleotide resolution for protein, metabolic and genome engineering. *Nat. Biotechnol.* **35**, 48–55 (2017).
45. Lian, J., Schultz, C., Cao, M., HamediRad, M. & Zhao, H. Multi-functional genome-wide CRISPR system for high throughput genotype-phenotype mapping. *Nat. Commun.* **10**, 5794 (2019).
46. Elkins, C. A. & Nikaido, H. Substrate specificity of the RND-type multidrug efflux pumps AcrB and AcrD of *Escherichia coli* is determined predominantly by two large periplasmic loops. *J. Bacteriol.* **184**, 6490–6498 (2002).
47. Lennen, R. M., Politz, M. G., Kruziki, M. A. & Pfleger, B. F. Identification of transport proteins involved in free fatty acid efflux in *Escherichia coli*. *J. Bacteriol.* **195**, 135–144 (2013).
48. Park, W. S. et al. Combinatorial metabolic engineering strategies for the enhanced production of free fatty acids in *Escherichia coli*. *J. Agric. Food Chem.* **70**, 13913–13921 (2022).
49. Huang, M. et al. FACS-based genome-wide CRISPR screens define key regulators of DNA damage signaling pathways. *Mol. Cell* **83**, 2810–2828 (2023).
50. Menasche, B. L. et al. Fluorescence activated cell sorting (FACS) in genome-wide genetic screening of membrane trafficking. *Curr. Protoc. Cell Biol.* **82**, e68 (2019).
51. Xu, P., Qiao, K., Ahn, W. S. & Stephanopoulos, G. Engineering *Yarrowia lipolytica* as a platform for synthesis of drop-in transportation fuels and oleochemicals. *Proc. Natl Acad. Sci. USA* **113**, 10848–10853 (2016).
52. Cai, P. et al. Methanol biotransformation toward high-level production of fatty acid derivatives by engineering the industrial yeast *Pichia pastoris*. *Proc. Natl Acad. Sci. USA* **119**, e2201711119 (2022).
53. Yu, T. et al. Reprogramming yeast metabolism from alcoholic fermentation to lipogenesis. *Cell* **174**, 1549–1558 (2018).
54. Gao, J. et al. Engineering co-utilization of glucose and xylose for chemical overproduction from lignocellulose. *Nat. Chem. Biol.* **19**, 1524–1531 (2023).
55. Kim, H. M., Chae, T. U., Choi, S. Y., Kim, W. J. & Lee, S. Y. Engineering of an oleaginous bacterium for the production of fatty acids and fuels. *Nat. Chem. Biol.* **15**, 721–729 (2019).
56. Datsenko, K. A. & Wanner, B. L. One-step inactivation of chromosomal genes in *Escherichia coli* K–12 using PCR products. *Proc. Natl Acad. Sci. USA* **97**, 6640–6645 (2000).
57. Bikard, D. et al. Programmable repression and activation of bacterial gene expression using an engineered CRISPR-Cas system. *Nucleic Acids Res.* **41**, 7429–7437 (2013).
58. Cao, Y. X. et al. Heterologous biosynthesis and manipulation of alkanes in *Escherichia coli*. *Metab. Eng.* **38**, 19–28 (2016).
59. Zhang, F., Carothers, J. M. & Keasling, J. D. Design of a dynamic sensor-regulator system for production of chemicals and fuels derived from fatty acids. *Nat. Biotechnol.* **30**, 354–359 (2012).
60. Love, M. I., Huber, W. & Anders, S. Moderated estimation of fold change and dispersion for RNA-seq data with DESeq2. *Genome Biol.* **15**, 550 (2014).
61. Cox, J. & Mann, M. MaxQuant enables high peptide identification rates, individualized p.p.b.-range mass accuracies and proteome-wide protein quantification. *Nat. Biotechnol.* **26**, 1367–1372 (2008).
62. Bruderer, R., Bernhardt, O. M., Gandhi, T. & Reiter, L. High-precision iRT prediction in the targeted analysis of data-independent acquisition and its impact on identification and quantitation. *Proteomics* **16**, 2246–2256 (2016).
63. Choi, M. et al. MSstats: an R package for statistical analysis of quantitative mass spectrometry-based proteomic experiments. *Bioinformatics* **30**, 2524–2526 (2014).
64. Livak, K. J. & Schmittgen, T. D. Analysis of relative gene expression data using real-time quantitative PCR and the 2(-Delta Delta C(T)) Method. *Methods* **25**, 402–408 (2001).
65. Rosenberg, M. Microbial adhesion to hydrocarbons: twenty-five years of doing MATH. *FEMS Microbiol. Lett.* **262**, 129–134 (2006).

Acknowledgements

This work was financially supported by the National Key Research and Development Program of China (2021YFC2104400, Y. Cao), the National Natural Science Foundation of China (22478294, Y. Cao, 22308256, L.F.), and the China Postdoctoral Science Foundation (2024T170643, L.F.).

Author contributions

L.F. and Y. Cao conceived the study. L.F., X. Hao, and J.F. designed and performed most of the experiments. X.L., Y. Chen, and L.W. assisted with fermentation and data analysis. X. Huang assisted with figure creation and layout. L.F. and Y. Cao analyzed the data and wrote the manuscript. Y. Cao and H.S. supervised all aspects of the study. Y. Cao and L.F. funded the study. All authors approved the manuscript.

Competing interests

Y. Cao, L.F., X. Hao, and H.S. have filed two provisional patents no. CN118667851A and CN118667850A, which include the construction methods and applications of the *pcnB*^{i} and *pcnB*^{i}-*acrD*^{i}-*fadR*$^{+}$ strains for FFAs production. The remaining authors declare no competing interests.

Additional information

Supplementary information The online version contains supplementary material available at https://doi.org/10.1038/s41467-025-58368-3.

Correspondence and requests for materials should be addressed to Yingxiu Cao.

Peer review information *Nature Communications* thanks Mattheos Koffas, Yu-Ping Shen, and the other, anonymous, reviewer(s) for their contribution to the peer review of this work. A peer review file is available.